Lawrence Berkeley National Laboratory
Recent Work

Title
ELECTRON DAMAGE and DEFECTS IN ORGANIC CRYSTALS

Permalink
https://escholarship.org/uc/item/7696d19b

Author
Howitt, David George.

Publication Date
1976-06-01

eScholarship.org Powered by the California Digital Library
University of California

0 0 0 0 4 5 0 0 9 3 5

LBL-4979

ELECTRON DAMAGE AND DEFECTS IN ORGANIC CRYSTALS

RECEIVED
LAWRENCE
BERKELEY LABORATORY
OCT 19 1976
LIBRARY AND
DOCUMENTS SECTION

David George Howitt
(Ph. D. thesis)

June 1976

Prepared for the U. S. Energy Research and
Development Administration under Contract W-7405-ENG-48

For Reference

Not to be taken from this room

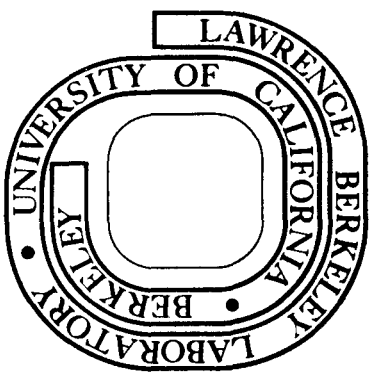

LBL-4979

DISCLAIMER

This document was prepared as an account of work sponsored by the United States Government. While this document is believed to contain correct information, neither the United States Government nor any agency thereof, nor the Regents of the University of California, nor any of their employees, makes any warranty, express or implied, or assumes any legal responsibility for the accuracy, completeness, or usefulness of any information, apparatus, product, or process disclosed, or represents that its use would not infringe privately owned rights. Reference herein to any specific commercial product, process, or service by its trade name, trademark, manufacturer, or otherwise, does not necessarily constitute or imply its endorsement, recommendation, or favoring by the United States Government or any agency thereof, or the Regents of the University of California. The views and opinions of authors expressed herein do not necessarily state or reflect those of the United States Government or any agency thereof or the Regents of the University of California.

0 0 0 0 4 5 0 3 9 3 6

LBL 4979

ELECTRON DAMAGE AND DEFECTS IN ORGANIC CRYSTALS

by

David George Howitt

Lawrence Berkeley Laboratory
University of California
Berkeley, California 94720

0 0 0 0 4 5 0 3 9 3 7

TO THE MEMORY OF MY MOTHER

0 0 0 0 4 5 0 3 9 3 8

CONTENTS

0 0 0 0 4 5 0 3 9 3 9

ELECTRON DAMAGE AND DEFECTS IN ORGANIC CRYSTALS

David George Howitt

Materials and Molecular Research Division, Lawrence Berkeley Laboratory
and Department of Materials Science and Engineering,
University of California, Berkeley, California 94720

ABSTRACT

The nature of the defects discernable from, and the radiation damage that is induced by, high resolution electron microscopy is reported.

It has been shown that it is possible to correlate the structural aspects of the radiation damage process to the expected radiochemical decomposition of these materials and to identify these effects. It has also been shown that the types of local defect formed by radiation damage are often clearly distinguishable, in high resolution images, from those inherent in the microstructure.

The particular techniques used in this type of electron microscopy and the limitations imposed by radiation damage are described as are the relevant radiochemical characteristics of these processes.

In copper pthalocyanine microstructural features distinct from those induced by radiation damage have been identified which are consistent with those predicted and described by other workers in similar materials. The high resolution studies indicate that some of the microstructures observed are caused by structural rearrangements that can account, to some extent, for additional crystallographic forms that have been identified in this material and the photochemical behaviour of related structures.

The purpose of this study was to demonstrate that it is possible for high resolution electron microscopy to play a significant role in the structural investigations of organic materials.

0 0 0 0 4 5 0 3 9 4 0

I. ELECTRON MICROSCOPY AND ORGANIC MATERIALS

A. Introduction

The application of the techniques of electron microscopy to the study of crystalline organic materials is severely restricted by the phenomenon of radiation damage, which is induced in these materials by the electron beam. Under conditions of experimental analysis this radiation damage is encountered as a rapid loss of specimen mass and crystallinity, which become more pronounced as the electron exposure continues.

This situation is hardly an attractive one and since no solution to the radiation damage problem can be found, the attempts at microscopy in these materials are often only token studies.

The purpose of the investigation described here was to comprehensively examine some organic materials in the electron microscope and to attempt to identify their microstructures at high resolution before they were destroyed by the radiation damage. A study such as this necessarily requires an investigation of the effects of radiation damage and an assessment of the factors appropriate to its induction in the electron microscope.

The ways by which radiation damage can occur in these materials are considered in chapter II, however, it arises principally from the effects of ionization, caused by the high energy electron beam, which promote violent chemical reactions. The term ionization is in this case referring to both the ionization and excitation of molecules or atoms.

The radiation exposures of conventional 100kV electron microscopes are in fact extremely intense; the commonly used electron intensity of one ampere cm^{-2} when given to an organic specimen corresponding to approximately 400,000 Mega rads per second. Such an exposure is seldom encountered outside the electron microscope and is equivalent to the exposure received by an object thirty yards away from a series of 100 Megaton H bombs exploding at the rate of ten a second. Not surprisingly, therefore, radiation sensitive materials are not well suited to investigation by electron microscopy. In most organic materials the critical exposure, or dose to destroy the specimen, is rarely better than about $10^{-2} C\ cm^{-2}$ which corresponds to a specimen lifetime of 10^{-2} seconds at conventional intensity levels. The techniques of microscopy that can be used and the limitations that are involved in the study of these materials are the subjects of Chapter III.

In the event of the successful recording of micrographs, the problem of interpretation is not always trivial. The degree of radiation damage sustained, and its contribution to the results, is of course increased as the electron dose to record data approaches the critical exposure, however no structural significance can be attached to intermediate values of this dose. The nature of the progression of radiation damage and its significance to the interpretation of electron micrographs is the subject of Chapter IV.

The microstructural analysis of one of the most radiation resistant organic materials (β-copper pthalocyanine) is the subject of Chapter V and here, at high resolution, it is possible to identify some of the

0 0 0 0 4 5 0 5 9 4 1

microstructures that have been predicted in other molecular organic materials and to account for some anomolies also.

B. The Materials Studied

The materials employed in this investigation were the aliphatic amino acid l-valine, the pyrimidine cytosine, in its hydrated and anhydrous forms and the metalo-organic aromatic copper pthalocyanine. These materials have respective critical exposures of 3×10^{-3}, 1×10^{0}, 4×10^{-2} and 3×10^{0} Ccm^{-2} to 100kV electrons and are all molecular organic compounds. All the materials studied are therefore monomeric in structure with the molecules in the lattice being held together by hydrogen bonds and van der Waals forces. The structures of all the materials have been determined by X-ray analysis (Torri and Iitaka 1970; Jeffrey and Kinoshita 1961; Barker and Marsh 1964; Robertson 1935) and all but the anhydrous form of cytosine which is primitive orthorhombic, are primitive monoclinic. The space groups and lattice parameters of these materials are listed in Table I-I. The molecular compositions and arrangements of the molecules in the crystal lattices are shown in figures 1-1, 1-2 and 1-3, where the projections of the three dimensional structures represent views along stacked rows of molecules which project out of the plane of the drawings. An alternative method to visualize these complicated structures is to consider the molecules of different orientation in the lattice as separate units. The copper pthalocyanine structure therefore could be envisaged as an ordered array of distinguishable molecules in a C centered monoclinic

unit cell, with molecules of type A at the cell corners and molecules of type B at the centers of the C faces. This type of approach to these structures is particularly useful when characterizing their microstructures, since it emphasizes the molecular arrangements.

0 0 0 0 4 5 0 3 9 4 2

Table I-1 The Lattice Parameters and Space Group Symmetries of the Materials Studied.

Material	a	b	c	α	β	γ	Space Group
l-valine	9.71Å	5.27Å	12.06Å	90°	90.8°	90°	$P2_1$
cytosine	13.04Å	9.49Å	3.82Å	90°	90°	90°	$P2_12_12_1$
cytosine monohydrate	7.80Å	9.84Å	7.68Å	90°	99.7°	90°	$P2_{1/c}$
copper pthalocyanine	19.6Å	4.79Å	14.6Å	90°	120.6°	90°	$P2_{1/a}$

FIGURE CAPTIONS

Fig. I-1 The projection of the crystal structure of l-valine along the b axis is shown in (1) whilst a stereoscopic drawing of the same projection of a single layer is shown in (2). The chemical structure of l-valine is shown in (3).

Fig. I-2 The projection of the crystal structure of cytosine along the c axis is shown in (1) whilst a projection of the crystal structure of cytosine monohydrate perpendicular to the b and c axes is shown in (2). In (2) the lone oxygen atoms represent water molecules which lie roughly in the plane of the cytosine molecules. The chemical structure of cytosine is shown in (3).

Fig. I-3 An orthographic projection of the crystal structure of β-copper pthalocyanine is shown where (1) is a view down the b axis, (2) is a view down the a axis, (3) is a view down the c axis and (4) is a view perpendicular to the a and b axes. (5) is the structure of the molecule which is represented by the projected squares in the Fig. The central square of the molecule represents the copper atom, the open circles the carbon atoms and the closed circles the nitrogen atoms.

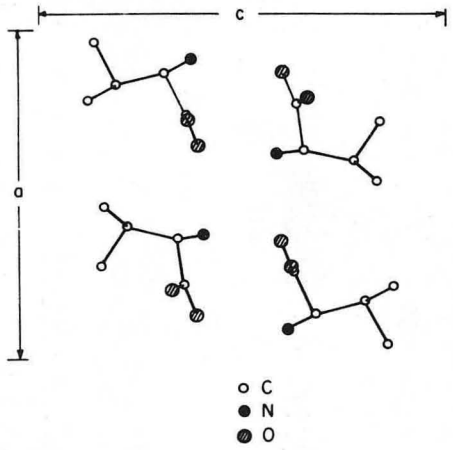

(1)

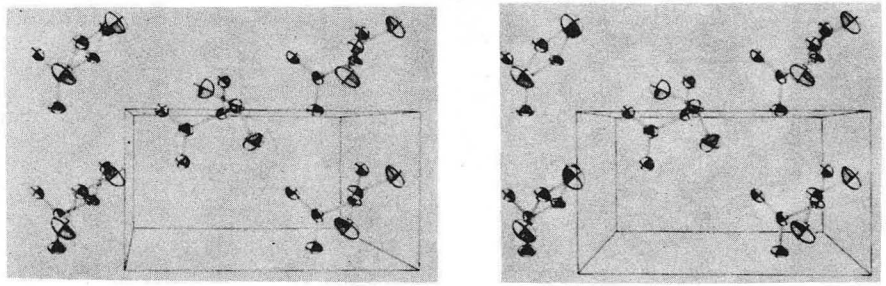

(2)

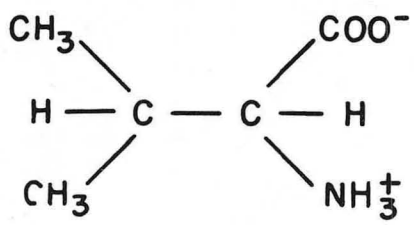

(3)

XBB765-4437

Fig. 1-1

0 0 0 4 5 0 3 9 4 3

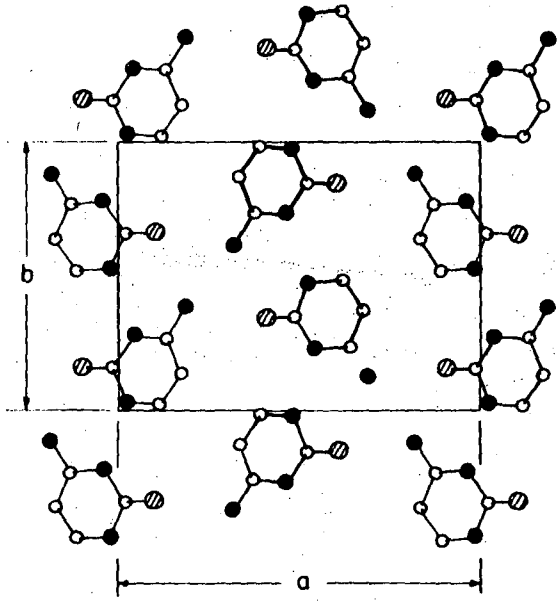

(1)

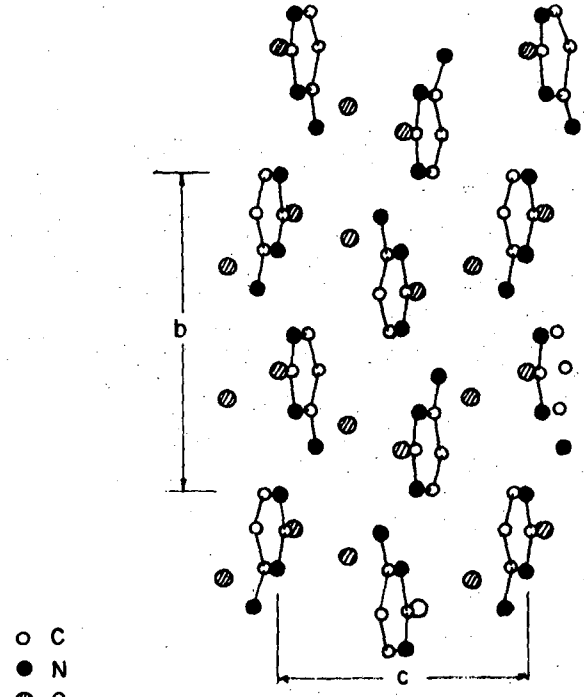

(2)

○ C
● N
▨ O

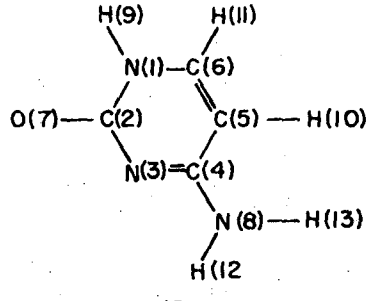

(3)

XBL 765-1883

Fig. 1-2

0 0 0 0 4 5 0 3 9 4 4

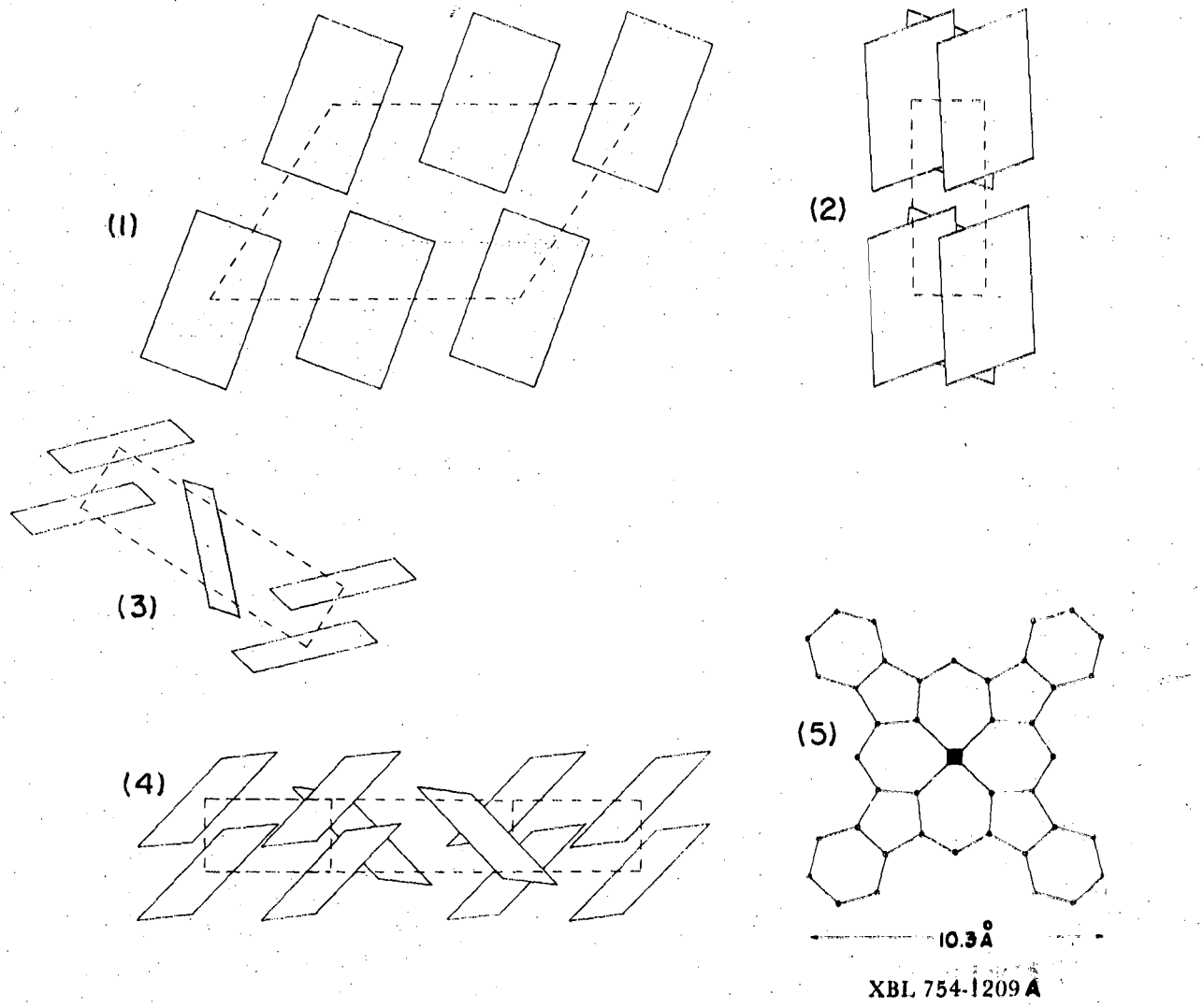

Fig 1-3

II. RADIATION DAMAGE IN ORGANIC MATERIALS

A. The Radiation Damage Processes

In the electron microscope organic materials can undergo radiation damage via the processes of ionization or direct atomic displacement, the magnitude of the respective contributions being dependent upon the material's composition, its structure and the energy of the incident electrons. These two processes are energetically somewhat different since in the case of direct displacement, where the atom rather than the electron is the target, momentum conservation imposes a severe restriction on the amount of energy that can be transferred from the impinging electron. The maximum energy transfer from a 100keV electron in a displacement collision with a hydrogen atom is only about 200 eV, whilst half the incident electron's energy can be transferred to an atomic electron in an ionization event. In addition, since the energy transfer necessary for displacement is about 2 eV, only electrons with energy greater than about 1keV are capable of affecting displacement damage, whilst electrons of only a few eV can affect ionization. This difference is significant, since the degree to which secondary electrons can effect the damage process will be very much larger for ionization and will greatly increase the overall probability of such an event occuring in the specimen. The probability of an ionization event (Howitt, 1974), even without this correction, is some four orders of magnitude larger than a displacement event for 100kV electrons (Seitz and Koehler, 1956) and hence the contribution from direct displacement processes is usually small.

0 0 0 0 4 5 0 3 9 4 5

Similarly, and because the energy transfer to a displacement event is small, the total energy lost to the specimen by the electron beam is almost entirely consumed by ionization events. In penetrating carbon a 100keV electron will on the average lose ∿833 eV/μ (Berger and Seltzer, 1964); a value that remains constant for the first ten microns in this material and corresponds to some 16 ionizations/μ (Rauth and Simpson, 1964). The effect of high energy secondary electrons escaping the sample will tend to reduce this value as the specimen thickness is decreased and as the energy of the incident electrons is increased. Alternatively the additional energy losses from Bremstrahlung (radiation losses), and the interaction of the resulting electromagnetic radiation with the specimen, will tend to increase the radiation damage process at very high electron energies (>10MeV) and as the specimen thickness is increased. The possibility of a Bremstrahlung contribution to the radiation damage process at 100keV is however very small. In the first place the probability of these events is low (Bethe and Heitler, 1934), and in the second place the resulting hard X-rays are extremely penetrating in comparison to electrons of the same energy ($\sim 1/10^8$) and will interact to a proportionately smaller extent.

The radiation damage process resulting from direct displacement is simply caused by the rearrangement of atoms within the material, whilst the damage from ionization is more complicated involving subsequent chemical interaction of the ionized or excited species. The total probability of an ionization event followed by a subsequent chemical event is nevertheless much greater than the probability for

the more simple direct displacement event in most organic materials and it is the probability of these chemical interactions that determines the sensitivity of a particular material to radiation damage. The critical exposure is an inverse measure of this probability and in l-valine, a material that damages almost totally by ionization, the critical exposure at 100keV is $3.10^{-3} Ccm^{-2}$. In chlorine substituted pthalocyanine on the other hand, where the probability of chemical interaction is greatly suppressed, the critical exposure at 100 keV is $2.5 \times 10^{1} Ccm^{-2}$.

B. The Physical Effects of Radiation Damage

The processes of radiation damage that are induced in organic materials by fast electrons tend to distribute themselves firstly along the primary track of the electron and then, as the depth of penetration increases, along branching tracks, resulting from events caused by the secondary electrons.

The majority of the secondary electrons produced from a 100keV primary are incapable of producing direct displacement and so the events from this process tend to be confined to the primary track. In a 100Å thick carbon film only one such event will occur for every 20,000 incident 100keV electrons. These events involve the displacement of a single atom and its incorporation elsewhere in the structure to form a stable Frenkel pair.

Ionization events on the other hand will not be so confined to the primary track since they are prolifically produced by the secondary electrons. In a 100Å thick carbon film an ionization event will occur

0 0 0 0 4 5 0 3 9 4 6

for every 6 incident 100keV electrons.

In the collision of a primary electron, with the electrons of the specimen, secondary electrons are produced whose energies can vary from a few electron volts to half the energy of the primary. The secondaries which have sufficient energy to produce their own track, ($E \gtrsim 100$ eV), are referred to as δ-rays. In the case of complete absorption of the primary electron the subsequent interactions of the δ-rays account for almost half of the total ionization; even though only about 5% of the primary electron interactions generate such electrons (Newton, 1963). The majority of the primary electron interactions produce lower energy secondaries directly.

The radiation damage process characteristic of low energy secondaries is ionization clustering and these events are often referred to as spurs (Magee, 1951). A spur is thought to contain between one and five ions, two and ten excited molecules and about twenty unexcited molecules within a sphere of some 20Å in diameter. The fast electron track is therefore a string of spurs with branches from the δ-rays which are in turn also spurred and branched. The intensity of the spurs and branches will of course increase as the associated electron becomes less energetic, until its energy falls below the lowest electronic excitation potential. The behaviour of these remaining electrons is not well understood but their energy transfer is to the vibrational (∿0.1 eV) and rotational states (∿0.01 eV) of the molecules. These mechanical processes are not associated with radiation damage. At very low electron energies (0.1 eV) these processes are in competition with electron

capture by neutral molecules or positive ions. These processes, of which the former is most likely, respectively produce negative ions and highly excited molecules which are capable of contributing to the radiation damage process.

In the case of thin specimens in the electron microscope total absorption of the electrons does not occur and so the electron tracks will not all end inside the specimen. The range of a 100keV electron in carbon is about 100μ and the thickness of specimens in the electron microscope vary between about 50 and 1000Å. The total track from the primary electron is therefore truncated. This does not however preclude the possibility of some electron tracks ending inside the specimen.

C. The Chemical Effects of Radiation Damage

The mechanisms by which the ionized and excited molecules in the specimen decay from their excited states determines the local structure of the radiation damage and the chemical products that form.

In general all the possible excited states of the molecules can be achieved and singly and doubly charged molecules are the result of direct ionization. Doubly charged molecules, which account for less than 10% of the ionized species (Newton, 1963), will either immediately fragment, into two singly charged daughter molecules, or exchange charge from one or both sites to yield two singly charged, but otherwise intact, parent molecules.

Singly ionized molecules can charge exchange with other molecules or fragment to form either a radical ion-radical pair, or a molecule ion-molecule pair, the latter requiring the formation of a double bond

0 0 0 0 4 5 0 5 9 4 7

in one of the species with the evolution of heat. Fragmentation of the ion species can continue or alternatively recombination with neutral molecules to create a different pair can follow. Alternative to the fragmentation is recombination with a slow electron to form a highly excited molecule which will decay in the same way as those created by collision.

The fate of the excited molecule also includes fragmentation, to yield radicals with excess kinetic energy, but in addition radiative decay, resulting in fluorescence and phosphorescence, vibrational decay or energy transfer to an adjacent molecule can occur.

The chemical processes which follow these events all involve the interaction of the ions and radicals, with either themselves, each other or with neutral parent or daughter molecules.

The broken bonds and reaction products that form need not arise from the least energetically stable portion of the molecules since many of the active species are held firmly in the lattice, preventing their reaction and forcing them to recombine. This "cage" effect in solids is often the deciding factor as to the nature of the final products formed.

D. The Characteristics of Radiation Damage in Selected Materials

1. Amino Acids (l-valine)

The radiation damage of amino acids in the dry state is almost entirely due to ionization damage. The site of main attack in these molecules is principally determined by the length of the carbon chain and in l-valine such fragmentation of the molecule is thought to occur

across the amino and acid bonds, the degradation pathway being in the main via deamination and decarboxylation (Gejvall and Lofroth, 1975). The bulk of the molecule's skeleton should therefore be preserved at least during the early stages of irradiation. The structure and composition of l-valine are shown in fig. I-1.

2. Pyrimidines

The presence of the conjugated ring renders the pyrimidines more resistant to ionization damage than the aliphatic amino acids. In cytosine rupture across the C=O and C–NH_2^+ bonds would be expected first, followed by the C-H bonds and finally by the rupture of the ring itself (Hall, Bolt and Carrol 1963). The structure and composition of the anhydrous and monohydrated forms of cytosine are shown in fig. I-2.

3. Pthalocyanines

In these materials the C–H bond rupture in the outer conjugated rings produces the early breakdown of the crystal lattice whilst the centre of the indigo molecule, consisting of carbon and nitrogen atoms, is very stable (Reimer, 1965). The molecule therefore most likely radiation damages inwards from the outside, gradually removing the influence of the "cage" effect. The structure and composition of copper pthalocyanine is shown in fig. I-3.

0 0 0 0 4 5 0 3 9 4 8

III. THE REDUCTION OF RADIATION DAMAGE IN THE ELECTRON MICROSCOPE

A. Introduction

In order to reduce the radiation damaging effect of the electron microscope it is necessary to reduce the probability of an ionization event followed by a subsequent chemical interaction occuring in the specimen. The probability of ionization is chiefly controlled by the energy of the impinging electron rather than the composition of the specimen and it has been shown that the effectiveness of the electron beam to induce damage can be reduced by some 75% when electron beams with energies in excess of 500 keV are employed (Howitt Thomas and Glaeser 1975).

The suppression of the chemical aspects is, on the one hand, a question of specimen design in the sense that the beam sensitivity of materials can be reduced by the substitution of certain components. In this way charge exchange away from the most sensitive sites for fragmentation can be promoted, so that the tendency for radiative decay is enhanced. Similiarly the closer packing of molecules to enhance the cage effect and radical scavenging can be achieved by the simple addition of appropriate compounds. The addition of aromatic components, which apparently protect nearby species from attack without readily sacrificing themselves would be probably the most singly effective additive.

Alternatively the chemical aspects of radiation damage can be reduced by external modification of the specimen, the sandwiching of specimens between metallic films (Salih and Cosslett 1975) and using

frozen hydrated specimens (Taylor 1975) being two significant techniques. The mechanisms by which these techniques effect the radiation damage process is not well understood since apart from their ability to act in the same way as the chemical additives they also modify the interface between the specimen and the microscopes environment. In the case of thin specimens this interface cannot be ignored since the microscopes environment will effect the equilibrium of the chemical interactions that ensue. The hard vacuum of the microscope will for example tend to extentuate the formation of any gaseous products and it has been shown that the direct control of the microscopes environment can play an important role in the reduction of radiation damage (Parsons 1975).

B. The Techniques of Transmission Electron Microscopy

In the application of electron microscopy to the study of a specific material a limitation to resolution is imposed when the number of electrons required to record an image is greater than the number required to destroy the specimen. This limitation is conveniently expressed in the equation due to Glaeser (1971); $d \geq \frac{1}{c} \cdot \frac{5}{\sqrt{fNcr}}$

where d is the size of the object detail, c the contrast of the object feature, f the detection efficiency of the recording device and Ncr the critical exposure, is the number of electrons in unit area which will destroy the specimen. In any attempt to apply electron microscopy therefore all these parameters should be maximised. Greater contrast can be achieved by the correct choice of specimen thickness and the substitution of heavy elements which promote strong scattering from the specimen. Similarly the collection efficiency of the recording device should be evaluated and in the case of photographic emulsions

0 0 0 0 4 5 0 3 9 4 9

a balance between film speed, grain size and image magnification should be attained such that the resolution of the emulsion is no better than the expected image resolution.

At the present time photographic emulsions are undoubtably the most efficient recording device.

The value obtained for the possible resolution, after the contrast and recording efficiency have been maximised, will represent an upper limit experimentally since additional electron doses to the specimen may be involved in the establishing of conditions for a suitable recording to be made. The choice of experimental technique should therefore be one which involves a minimal exposure to the specimen before the recording is made.

The only microscopy techniques which do not involve exposure of the specimen to the beam, other than that required for recording, involve the restriction of the illuminating electron beam to adjacent portions of the specimen until the moment when recording begins (Willams and Fisher, 1970), the nearness of the adjacent portion of specimen controlling the degree to which imaging conditions can be approximated.

The methods by which the beam can be deflected are numerous however the principal difficulty encountered is control over the beam size itself. In the conventional electron microscope the diameter of a reasonably undivergent beam is some five microns at the specimen which does not represent a problem at low resolution. At 20,000 X magnification however this area covers the final screen and by 200,000 X it is a meter broad. In addition, at high magnifications, local specimen

instability to rapid changes in beam current become more of a problem and the periods of stabilization can be large in comparison to the periods of recording. The application of such techniques is therefore very difficult at high magnifications.

The problem of beam size and specimen stability have been overcome at high resolution, in this study, by employing a continual low electron incidence to the regions of interest and performing microscopy at these low levels of illumination. Typically the electron incidence rate is such that photographic exposures are of the order of forty to sixty seconds and hence the time to establish image conditions can be kept to less than half the period of a recording. The principal disadvantage of this technique is the large error involved in establishing the conditions appropriate to the image at these low intensity levels. The experimental technique used for moderate resolution studies was the condenser objective or Riecke mode (Reicke, 1969) where the incident area of illumination on the specimen is controlled by the size of the condenser aperture and is independent of condenser excitation. The principle of this mode is that using a Lorentz pole piece the objective lens can be strongly excited to make the plane of the second condenser aperture conjugate to the specimen. This technique has been exploited in the study of selected area diffraction since the definition of electron incidence is so high that the intermediate aperture can be dispensed with. This refinement is directly applicable to the study of beam sensitive materials since the conditions for imaging can be established, and the intensity of the beam decreased slowly, without

0 0 0 0 4 5 0 3 9 5 0

disturbing the regions of interest. The condenser aperture can then be translated to expose the desired regions for recording.

At present however the Lorenz pole piece cannot be introduced into the high resolution stages of most electron microscopes and hence the limitations to resolution are controlled by instrumental design.

C. Experimental Data

The specimens of all the materials examined were prepared on formvar coated copper grids which were subsequently vacuum deposited with carbon to prevent their charging in the beam.

Observations of the specimens were performed in both a Philips 301 and Siemens 102 electron microscope in the Reike and conventional transmission modes respectively.

The image and diffraction patterns from these crystals were recorded either on Kodak E.M. or Kodak no-screen x-ray film, the latter's emulsion being effectively seven times faster.

To minimise the electron exposures to the material the images were recorded at electron intensities of approximately 10^{-12} amperes cm^{-2} at the final image plane where magnifications of between 20,000 and 100,000 were used. Thus although these intensities involve exposures of approximately 20 seconds for the x-ray film the proportional electron exposure to the specimen during the operation of the microscope is reduced.

The recording of diffraction data for analysis was performed in the Reike mode at a proportionally lower beam current density to the specimen than for the image work, hence the effects of radiation damage

could be more nicely defined. The diffraction patterns were standardised by covering the specimens with a layer of evaporated gold and the image magnifications were calibrated directly from this diffraction data. In this way the lattice spacing could be measured directly using the superimposed spacing of known value.

The magnitude of the critical exposures for all the materials were made using a Faraday cup (Howitt, Thomas and Toutolmin, 1976). During experimental observations of these materials the exposure sustained by any crystal was determined as a fraction of its lifetime at the particular current density. In this way the electron doses to the specimen could be calculated without having to measure the beam intensities through the specimen.

The Kodak electron image plates and x-ray films were developed at room temperature using D19 and Kodak liquid x-ray developer respectively. No stop bath was used and development was continued to a visible level of background fog.

Diffraction patterns for all the materials examined were calculated from the crystallographic data from x-ray analysis.

0 0 0 0 4 5 0 3 9 5 1

IV. THE DIRECT OBSERVATION OF RADIATION DAMAGE IN ORGANIC MATERIALS

A. Introduction

In the study of organic materials by electron microscopy the effects of in-situ radiation damage to the specimen is always encountered to some extent. The susceptibility of a specific material to radiation damage is often expressed as its critical exposure, which can also be expressed in terms of an upper limit to resolution when the signal requirements of a statistically noisy image are considered (Glaeser, 1971) (Chapter III-B).

The studies of unstained organic materials, using techniques of electron microscopy, are therefore usually limited to the attainment of a particular resolution from the material, or the analysis of microstructural features where the required resolution for identification is well below the limit imposed by radiation damage. The assignment of this reliable resolution limit for a specific material is necessarily experimentally derived since the structural aspects of the radiation damage process are not well understood and the critical exposure refers to the loss of all resolvable detail.

The chemical and physical aspects of the radiation damage process, on the other hand, have been reasonably well characterized suggesting it should be possible to elucidate upon some of the structural aspects of the process by an investigation of the behaviour of organic materials under in-situ irradiation in the electron microscope. With this information it would then be possible to study these materials at higher resolution when the necessary dose levels are inducing significant radiation damage.

B. Results

The effects of in-situ irradiation in the electron microscope can be directly observed via three characteristic contrast phenomena. Firstly, as changes due to structure factor; secondly, as changes due to mass thickness; and thirdly, as changes due to differences in the local diffracting conditions (diffraction contrast).

The changes in structure factor contrast will arise since the structure factor is dependent upon the lattice parameters and point group configuration of the specimen. Any change in the point group configuration is evidenced as intensity changes in the fourier components contributing to the diffraction pattern and the image, whilst the lattice parameter fluctuations are evidenced as changes in their reciprocal and real space co-ordinates.

The changes in mass thickness or diffraction contrast are solely characteristic of the orientation and bulk dimensions of the specimen and are therefore best monitored in the image at moderate magnifications.

Experiments in diffraction upon the materials examined showed that the co-ordinates of many diffraction spectra were strongly radiation sensitive. With continued electron exposure, variations in the magnitude and direction of their associated reciprocal lattice vectors (g_{ij}) were observed, these variations being independent of the orientation of the specimen to the incident electron beam. This behaviour, which corresponds to a contraction or expansion of the associated lattice spacings in real space, cannot be so satisfactorily monitored in the images because of the small electron exposures ($\sim 10^{-4} Ccm^{-2}$)

0 0 0 0 4 5 0 3 9 5 2

needed to induce such changes. The magnitude of these variations in terms of the real space separation between lattice planes are given in Table IV-1 for all the materials. Examples of the diffraction data are shown in Figure IV-1 and lattice images from cytosine monohydrate showing their destruction with continued exposure is shown in Figure IV-2. A lattice image from the $(20\bar{1})$ planes of copper pthalocyanine after about 5% expansion is shown in figure IV-3 and the optical diffractogram indicating that the image still contains resolvable detail to about 3Å is also shown.

In copper pthalocyanine it was possible, at high resolution, to monitor the induction of radiation damage in the lattice images themselves. Examples of this radiation damage are shown in Figure IV-4. These images are distinct from the homogeneous fading of lattice images which was also observed, often with their reappearance in a later photograph (figure IV-5b).

The effects of mass loss is most conveniently monitored in this material by the disappearance of the sloping edges from this faceted material with increasing electron dose (figure IV-5a). In figure IV-6 the changes in the spacing of the $(20\bar{1})$ planes in copper pthalocyanine and the visible effects of radiation damage are correlated with dose.

C. Discussion

The structures and molecular configurations of all the materials studied, except copper pthalocyanine, have been determined directly from x-ray diffraction (Torri and Iitaka, 1970; Jeffrey and Kinoshita, 1961; Barker and Marsh, 1964).

The structure of β-copper pthalocyanine has been determined from an x-ray analysis by Robertson (1935) and the close similarity this material bears to the nickel derivative (Robertson and Woodward, 1937) enables the atomic positions within the crystal lattice to be defined with good accuracy. These atomic positions cannot be used directly because of an error in one of the transformation matrices used to convert from the molecular to monoclinic axes; however by employing the original coordinates from the fourier projection the correct monoclinic coordinates can be obtained.

The structures of all the materials are listed in table I-1 and from this data it is straightforward to calculate the expected diffraction patterns; however, in none of these materials was an exact correspondence found between this data and the electron diffraction patterns obtained.

In previous studies of copper pthalocyanine (Menter, 1956) certain spacing inconsistencies were observed in the images, and were assigned to the projection of the $(20\bar{1})$ planes differing from their actual value of 9.6Å, being closer to values between 10.3 and 13Å. Thus in reciprocal space this effect was explained in terms of the strong shape factor from the reflection intersecting the Ewald sphere. The magnitude of these deviations is, however, too large to be accounted for by this phenomenon, involving rel-rods of $\sim 0.1 Å^{-1}$ and deviations from the Bragg condition of 30° or more.

The results obtained in this study indicate that in copper pthalocyanine, as well as in the other materials, the spacing variation

0 0 0 0 4 5 0 3 9 5 3

is electron dose dependent and can be monitored with increasing total exposure from the electron beam (figure IV-6).

Tilting experiments were also performed in these materials and no significant deviation in spacing was observed other than that due to the electron exposure, which can be readily confirmed by returning to the original orientation.

The consistency in the variations and the associated dependence upon electron exposure therefore indicate that these changes in lattice spacing are in fact due to the radiation damage process and that they are associated with the degradation of the crystal lattice. The exact molecular and crystal structure to which these materials degrade could not be determined exactly because of the difficulty associated with inducing the same degree of radiation damage in all the necessary crystal orientations.

An indication of the nature of this degradation can however be obtained by indexing the new diffraction patterns in the consistent notation of the perfect structure. This can be achieved by recording successive diffraction patterns, where the earliest recording can be unambiguously identified (figure IV-1b). Thus, by associating these indices with the more heavily irradiated patterns a new structure based on the same bravais lattice, can be identified as long as two dimensional periodicity is present.

The end point, where the radiation damaged structure has been identified in these materials, is identified at the electron dose to destroy two dimensional diffraction. In all the materials except

copper pthalocyanine the symmetry of the diffraction patterns obtained were such that this dose represented the critical exposure of the material.

In copper pthalocyanine however the diffraction patterns always sustain a single line of low resolution reflections which degrade less rapidly than the other higher resolution reflections that are initially present (e.g. figure V-1a). The induced structural changes in copper pthalocyanine, that are cited here, are calculated from the measurements made at the loss of two dimensional diffraction. These final values of the spacings of specific reflections are shown in Table IV-1.

The best fit data from these calculations are also shown in Table IV-1 for all the materials, compared to the data from x-ray diffraction.

In copper pthalocyanine it is apparent that a contraction in the <001> direction by some 7% occurs with a compensating expansion in the <100>direction by some 17%, there being a small variation along <010> of about 2%. This corresponds to a unit cell expansion of some 18%.

This behaviour is consistent with the structure of this material since the primary effects of radiation damage are associated with the outer conjugate rings of the molecule (Chapter II-D). These rings are not uniformly distributed about the molecule (Fig. 1-3) but are of maximum density at the corners of the projected squares. Loss of these outer rings would cause the unit cell to contract along the c axis and in the absence of mass loss or product escape from the crystal

0 0 0 0 4 5 0 3 9 5 4

surfaces the disordered array of radiation damage products would tend to increase the overall volume of the unit cell. That there is no notable expansion along the b axis suggests that these early radiation damage products distribute themselves very close to, or in the planes of the molecules and therefore arrange themselves around the remaining nitrogen cores.

From the evidence of the degradation of defect structures in this material (Chapter V), it appears that the pthalocyanine molecules of different orientation lose this distinction with continued irradiation. The degradation of the molecule may therefore be to a more symmetrical form itself or it may become more symmetrically oriented within the crystal lattice.

It is noteworthy that in platinum pthalocyanine the spacing anomaly was not observed by Menter; however, in this material the crystal morphology is such that in an untilted specimen the crystal pole is invariably within 2° of the <102> pole, considerably closer than in the copper derivative. Hence the strong $(20\bar{1})$ reflection which in copper varies in spacing by only 7%, is encountered in almost every crystal.

In anhydrous cytosine an overall contraction of the unit cell is observed. There is no detectable change in the b axis; the contraction being confined to the a and c axes. This behaviour correlates well with the expected early rupture of the C = O and C - NH_2^+ side groups since it is apparent from Fig. I-2(1), which represents a projection of the (001) planes of the structure, that these groups are closely

confined within the (001) planes. The invariance of the spacing of the (001) planes and the overall decrease in volume indicates that the damage products are probably escaping.

In cytosine monohydrate the effects of irradiation are much more marked. The contractions along the a and c axes are nearly by 30% with an unit cell volume contraction of over 50%. This apparently leads to difficulties in the accommodation of radiation damaged material in the parent matrix. Figure IV-2 is a sequence of consecutive micrographs of the (T11) (5.07Å) lattice images showing the breakdown of structure. This breakdown is already present in the first micrograph, but can be seen to be extending into the region of uniform contrast in the top right hand corner. Before the first micrograph was recorded the crystal displayed this type of uniform contrast over the whole surface. The cross hatched structure that develops is thought to be due to the local contraction of the specimen to form islands. These islands apparently separate from the body of the crystal along crystallographically preferred directions, resulting in a building block type structure. This behaviour is also evidenced by the development of the strong shape factor to the diffraction spots. These marked changes in structure are also apparent in other orientations exemplified by the <111> diffraction pattern of Fig. IV-1b.

The large contractions in cytosine monohydrate are thought to be due to the escape of water molecules which originally lie nearly within the (010) planes. Thus in Fig. I-2(2), which is a projection onto the (100) plane of the structure, the lattice is contracting both along

0 0 0 0 4 5 0 3 9 5 5

the c axis and a axis which is inclined out of the drawing. The a axis runs roughly out of the paper along the cytosine molecules and through the water molecules which are represented by the lone oxygen atoms. The loss of water from the structure is therefore consistent with the contraction of the a axis and since the water molecules are displaced out the molecular plane of the cytosine molecules by about 2Å along the c axis, it can account for this contraction also.

Despite this marked change of structure the overall effect of hydration in cytosine is to markedly increase the specimen's resistance to radiation damage, which is reflected in the respective critical exposures. The lattice images of cytosine monohydrate that were obtained involved extremely high radiation doses, for example, the dose received by the specimen before the first micrograph of Fig. IV-2 was recorded is about the critical exposure of the anhydrous derivative.

In l-valine the changes in lattice parameter can again be well correlated with the expected radiation damage. In this material the overall contraction is most prevalent along the c axis which is very close to the vector connecting the ends of adjacent molecules (Fig. I-3(l). The deamination and decarboxylation that is expected in this material, which would represent the removal of the nitrogen and oxygen atoms in (Fig. I-3(l), would contract the lattice predominantly along c.

In addition to the changes in lattice spacing the effects of radiation damage can be monitored by lattice imaging. Figure IV-4 shows two such lattice images, of the (001) ($\sim$ 12Å) planes of copper

pthalocyanine, from the same region of crystal but after different electron exposures. The second micrograph clearly shows the local destruction of the crystal lattice which bounds two regions of about 50Å in diameter. This dimension is of the same order of magnitude as that predicted for a spur (Magee 1951) (Chapter II-B).

This type of contrast should be distinguished from the fading of lattice images which are often thought to be indicative of uniform radiation damage. The sequence of lattice images in Fig. IV-5b, for example, displays such uniform fading with a subsequent return of the lattice images after continued irradiation. The effect in this case is thought to arise from changes in specimen thickness inducing changes in the contrast from the lattice images. This effect, whereby the contrast is maximised when the specimen thickness is an odd multiple of a quarter of the extinction distance (Hirsch et al 1965), was confirmed by monitoring the disappearance of the sloping edges from these cleaved crystals. These thinning edges are obvious in dark field (Fig. IV-5a), and also in the micrographs of Fig. IV-5b upon close inspection.

0 0 0 0 4 5 0 3 9 5 6

Table IV-1. The Crystallographic Data of the Radiation Damaged Materials

	Copper Pthalocyanine		Cytosine Monohydrate		Cytosine		l-Valine	
Reflection	1	2	1	2	1	2	1	2
001	12.57	12.4						
$20\bar{1}$	9.62	10.3						
100	16.88	21.0					9.71	8.9
010	4.79	4.9			9.49	9.4	5.27	4.9
110	4.61	4.8	6.06	4.6	7.67	7.6	4.63	4.2
$11\bar{1}$	4.54	4.6			3.42	3.5	4.33	4.9
$21\bar{1}$	4.29	4.3						
021	2.35	2.4						
210			3.58	2.5			3.57	3.2
011			6.00	4.5			4.82	4.3
$10\bar{1}$			5.92	4.5	3.66	3.7		
121			3.51	2.6				
$11\bar{2}$			3.42	2.6				
$\bar{2}1\bar{1}$			3.45	2.6				
a	19.6	22.9	7.801	5.6	13.041	12.8	9.71	8.9
b	4.79	4.9	9.844	9.8	9.494	9.3	5.27	4.9
c	14.6	13.6	7.683	5.4	3.815	3.8	12.06	9.2
β	120.6	113.7	99.7	111.2			90.8	90.0
Volume of the Unit Cell	1179.8Å^3	1397Å^3	581.6Å^3	276Å^3	472.3Å^3	452Å^3	617.2Å^3	401Å^3

1 = Original spacing in Å

2 = The average spacing in Å after radiation damage equivalent to the loss of two dimensional periodicity in diffraction, in all but copper pthalocyanine which corresponds to 0.7 Ccm^{-2}, this represents the critical exposure.

FIGURE CAPTIONS

Fig. IV-1 (a) Diffraction patterns from crystals of copper pthalocyanine in the <1$\bar{1}$0>. The micrograph showing two patterns a_3 is a double exposure of the same diffraction pattern after electron exposures of ~10^{-2} Ccm^{-2} and 1 Ccm^{-2} respectively. The difference in spacing of the respective (001) reflections represents a contraction of about 4%. The diffraction pattern where the gold rings are most obvious a_4 shows additional spots which are from an overlapping <102> pole with a common <010> axis.

(b) Diffraction patterns from cytosine monohydrate in the <111> pole showing the effects of radiation damage in the {1$\bar{1}$0} type reflections. The micrographs were recorded consecutively (1 through 4) from the same area of crystal at intervals equivalent to electron doses of 3×10^{-1} Ccm^{-2} at the specimen.

Fig. IV-2 Lattice images from the (T11) planes of cytosine monohydrate showing the breakdown of structure with radiation damage. The micrographs were recorded successively, each corresponding to an electron dose of approximately 3×10^{-1} Ccm^{-2} ((a) through (d)). The marker in d corresponds to 100 Å. The figure (a) has been magnified in (e) to show the (210) lattice images which were taken under conditions of tilted illumination.

Fig. IV-3 A lattice image and optical diffractogram from the (20$\bar{1}$) lattice images of copper pthalocyanine. The spacing of the

0 0 0 0 4 5 0 3 9 5 7

lattice images (10.3 Å) is 7% larger than the crystallographic data predicts. The optical diffractogram shows the image resolution to be better than 3.5 Å.

Fig. IV-4 Lattice images of the (001) lattice planes of copper pthalocyanine showing the effects of radiation damage. The micrographs are from the same region after electron exposures of $\sim 5 \times 10^{-1}$ Ccm (a) and 1 Ccm^{-2} (b).

Fig. IV-5 (a) A dark field $(20\bar{1})$ micrograph of copper pthalocyanine showing the strong contrast from the cleaved edges of the crystal which are inclined to the foil plane.

(b) Lattice images from the $(20\bar{1})$ planes of copper pthalocyanine displaying contrast fluctuations with continued electron exposure. The micrographs were recorded successively each requiring an electron dose of approximately 2×10^{-1} Ccm^{-2} with intervals equivalent to the same dose between them.

Fig. IV-6 The dependence of the spacing of the $(20\bar{1})$ lattice planes in copper pthalocyanine to electron exposure.

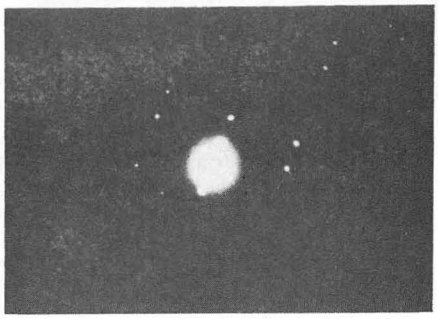

a 1

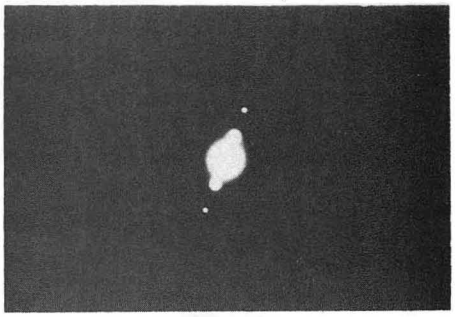

a 2

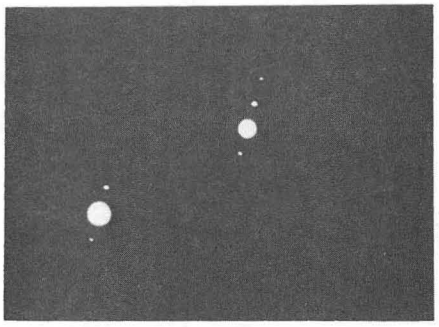

a 3

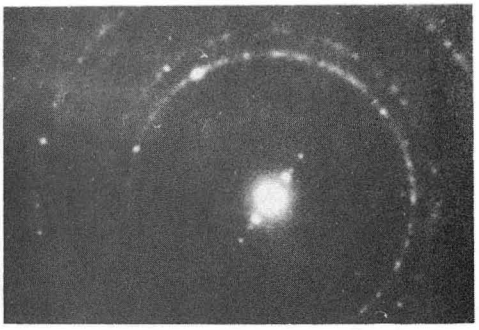

a 4

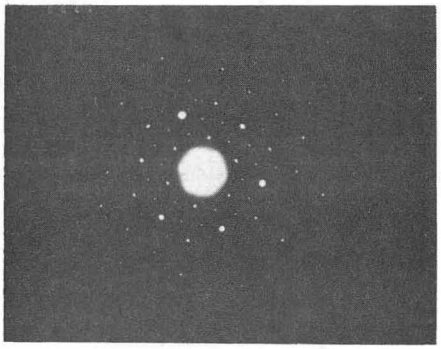

b 1

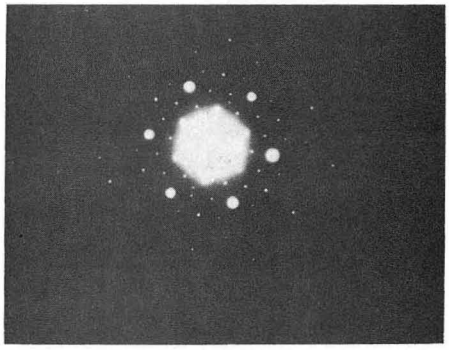

b 3

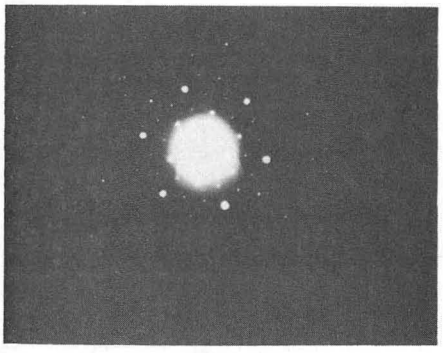

b 2

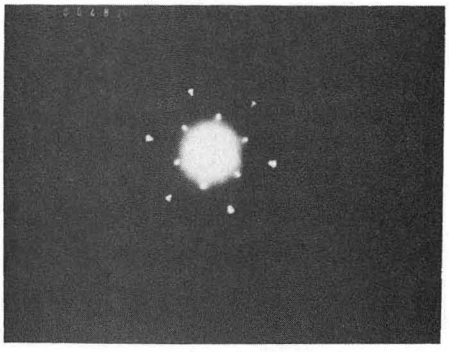

b 4

XBB-758-5823-A

Fig. 1V-1

0 0 0 0 4 5 0 3 9 5 8

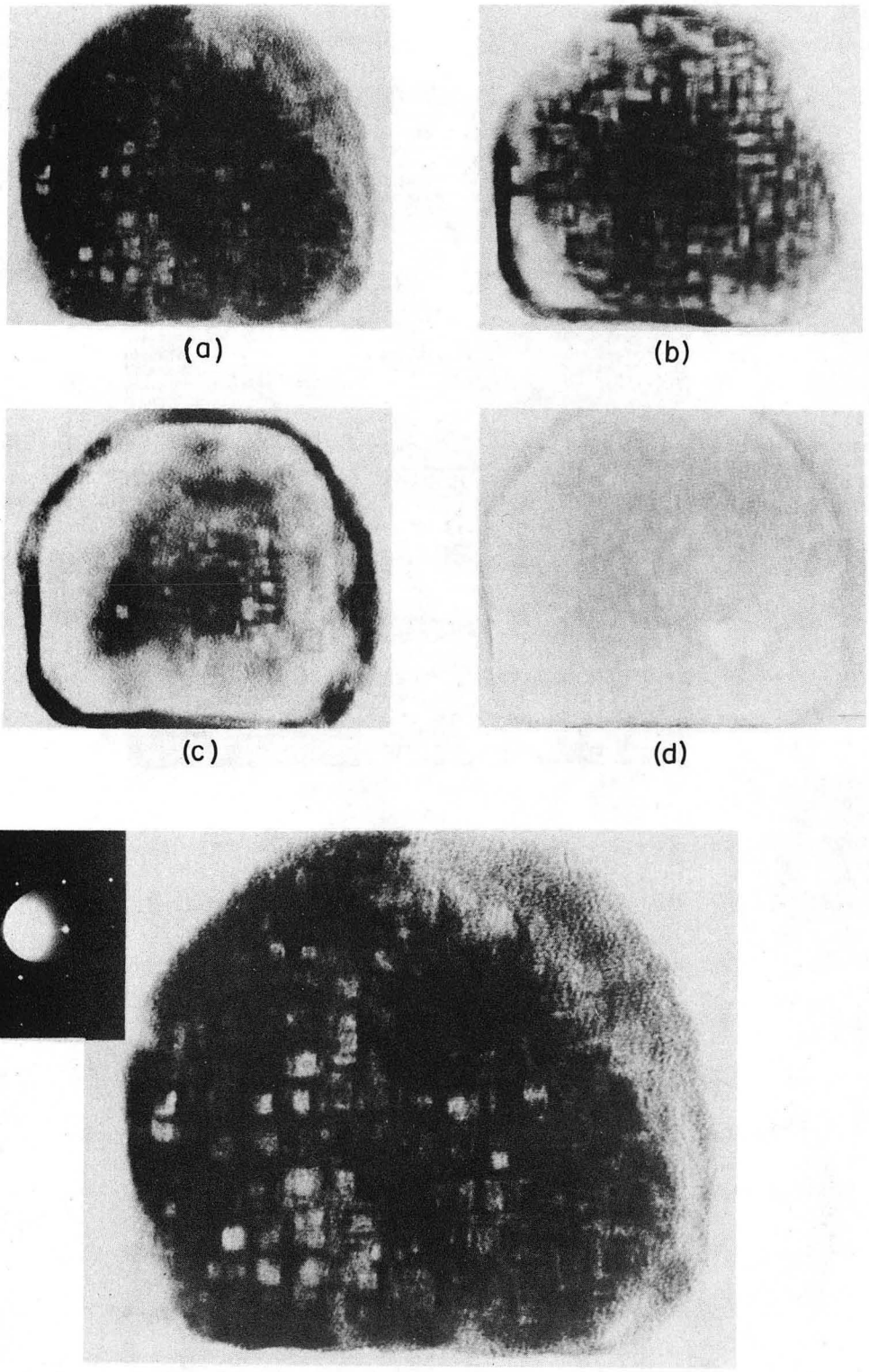

XBB765-4593

Fig. 1V-2

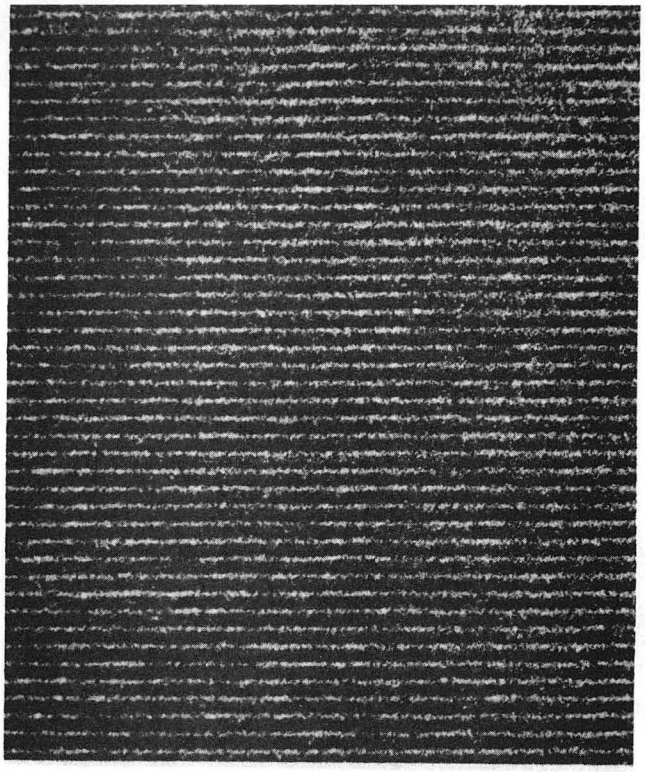

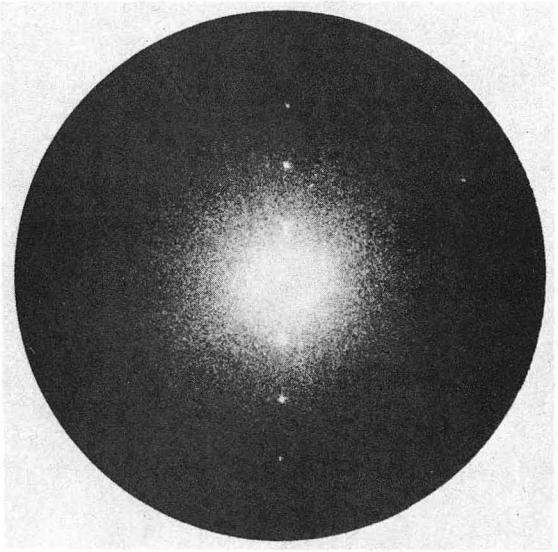

XBB744-2656A

Fig. 1V-3

0 0 0 0 4 5 0 3 9 5 9

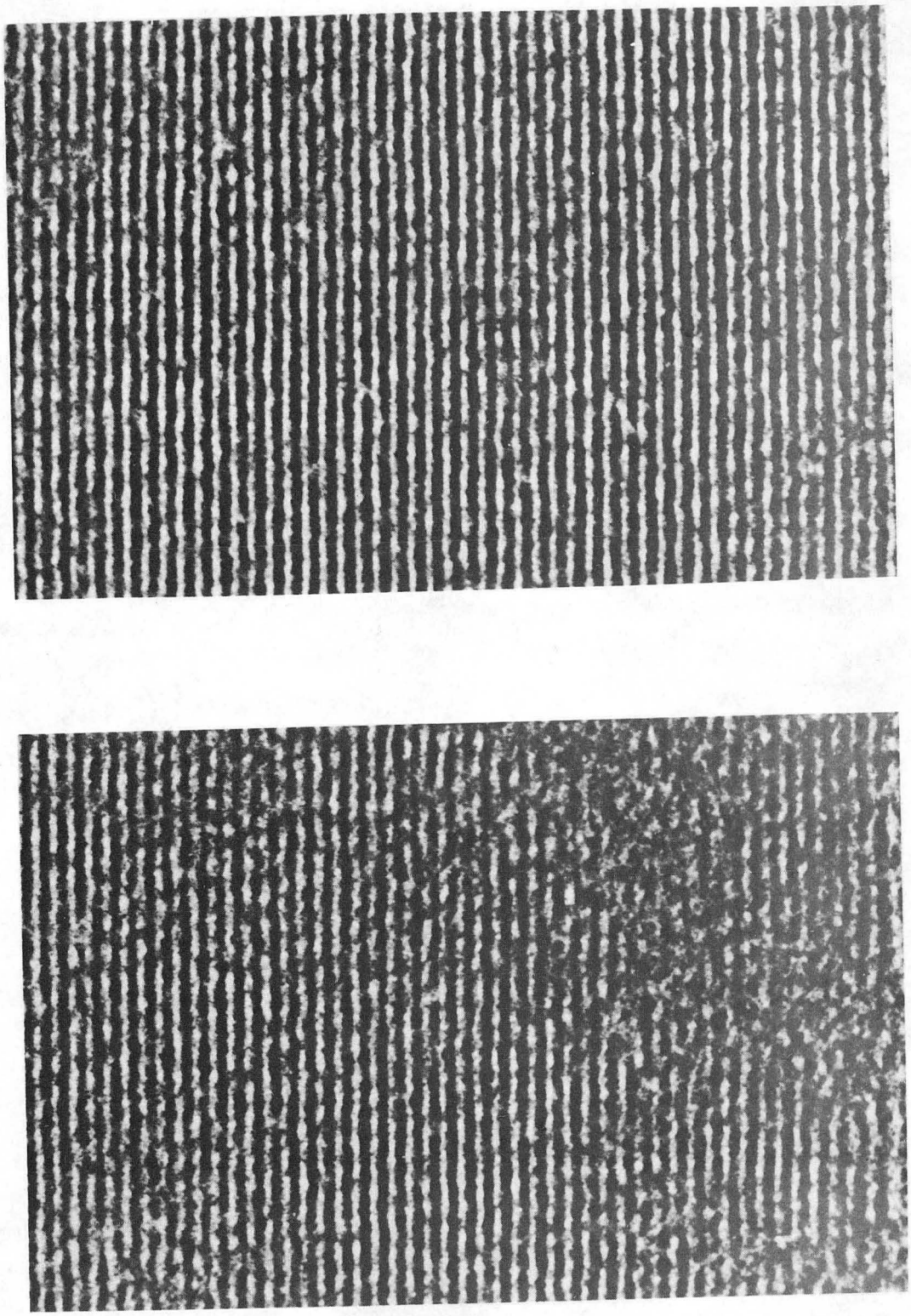

XBB744-2159

Fig. 1V-4

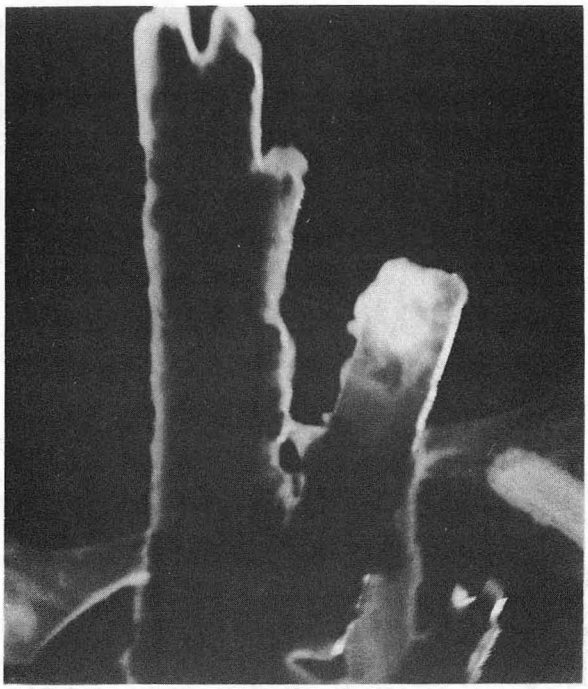

(a)

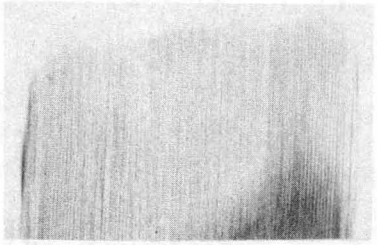

(b_1)

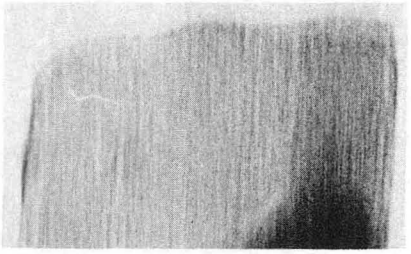

(b_2)

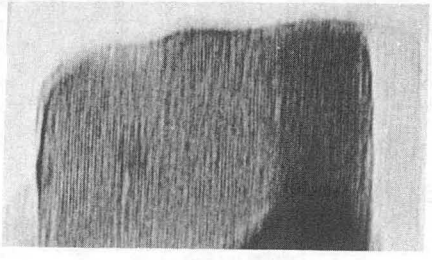

(b_3)

XBB765-4594

Fig. IV-5

0 0 0 0 4 5 0 3 9 6 0

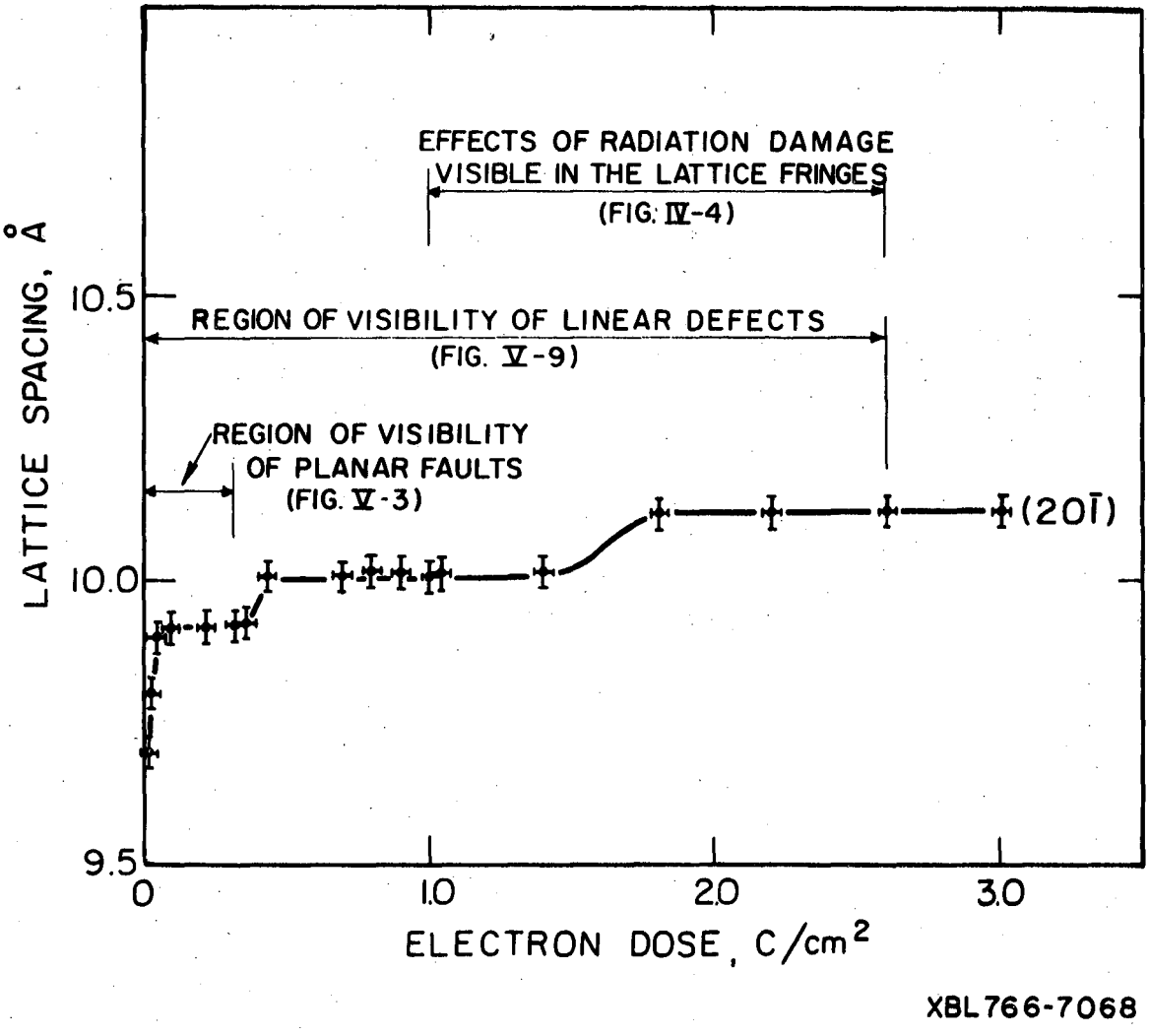

FIG. 1V-6

V. THE OBSERVATION OF DEFECTS IN COPPER PTHALOCYANINE

A. Introduction

In crystalline molecular organic materials there is good evidence to presuppose the presence of defects similar to those already confirmed in metallic crystals (Thomas and Williams 1972). The direct confirmation of these defects by electron microscopy is however severely hindered by the radiation damage sustained by these materials under electron exposure.

The techniques that can be employed for the examination of crystal defects in electron microscopy are high resolution lattice imaging and low resolution deficiency contrast (bright field) techniques of which the latter have been most popular.

The advantage of the low resolution techniques in the study of beam sensitive materials is of course from the smaller electron dose necessary to record an image, this dose increasing as the square of the linear magnification. The disadvantage is that since only one image can be recorded at a time and that in the analysis of some defects many different two-beam conditions are required, the complete analysis may involve a total exposure greater than that to record one high resolution micrograph. Indeed if the high resolution micrograph is a multibeam image it may be possible to determine the nature of a defect from such a single recording.

The limit to the information obtainable from either of these techniques, in a specific material, can of course be estimated from its critical exposure. However, it is possible that the contrast from

0 0 0 0 4 5 0 3 9 6 1

the defect will be lost at a dose considerably smaller than that required to destroy the long range crystal structure (Chapter IV).

Of the materials employed in this study, the most appropriate for microstructural investigation was copper pthalocyanine; firstly because of its large critical exposure but also because it does not drastically change its structure under such an electron dose. Furthermore, this material bears a structural similarity to the anthracene derivatives, upon which most of the indirect and low resolution defect analyses have been done (Thomas, 1974; Desvergne, Thomas, Williams and Bouas-Laurent, 1974; Jones, Thomas, Williams and Hobbs, 1975) and since the lattice spacings are quite large it affords the opportunity to study defects in this class of materials at high resolution.

In the interpretation of the results from any electron microscopy investigation, especially at high resolution, it is important to be able to distinguish between heterogeneities inherent in the microstructure and those induced by irradiation. It is necessary therefore to compare consecutive micrographs taken under identical conditions and to identify any heterogeneity which becomes more prevalent with continued irradiation.

In copper pthalocyanine the earliest stages of radiation damage are associated with an expansion of the unit cell (Chapter IV) and the induction of heterogeneities within the microstructure, certainly those that appear in the (001) and $(20\bar{1})$ lattice images, are in general confined to the latter stages of the materials degradation when the electron dose is in excess of 1 C cm^{-2}.

Thus by studying the lattice images of a material during the very early stages of radiation damage, microstructural information can be positively identified. The effects of radiation damage upon the behaviour of the defects themselves can also be significant since some of the predicted defects rely on the distinguishableness of molecules of different orientation, which may be destroyed more rapidly than the molecular framework. In the studies performed here microstructural features consistent with both modification to the original β-crystalline form of copper pthalocyanine and a transformation to a different crystal structure have been observed.

B. Results

From the high resolution lattice images of copper pthalocyanine two distinct structural modifications of the standard β-form have been identified. Neither of these modifications, or faulted versions of the β-form, have direct counterparts in metallic systems although their mechanisms of formation may be closely related to those known to occur in such systems.

The characteristics of these faults are that at high resolution they display both lattice images and diffraction spots characteristic of twice the spacing of a fundamental reflection, which cannot be interpreted in terms of the original structure. These transformed regions sustain an unique orientation relationship to the parent phase, in conflict with the results obtained by Mnyukh (1963) and Kilargorodsky (1965, 1975) who found that such orientation relationships between phases do not usually exist in organic crystals. Indeed the orientation

0 0 0 0 4 5 0 3 9 6 2

relationship between both the structures observed and the parent matrix is one of direct correspondence, where their diffraction patterns superimpose exactly except for the additional reflections (Fig. V-1a).

The additional reflections are thought to arise in both cases from a change in the nearest neighbor configuration of the molecules. In this way the stacking sequence is changed from one of regular spacing to one of alternate large and small spacing such that the separation of these low index planes is no longer a monorepeat sequence but is an alternate repeat sequence. Since an alternate repeat sequence has only the periodicity of the sum of the two spacings this is the new periodicity that is observed and being constrained in the parent matrix it would correspond to twice the average spacing of its surroundings.

The first example of this type of fault is the (001) type which includes the $(00\frac{1}{2})$ (25.1 → 23.4Å) reflection (referred to the coordinates of the perfect crystal). Representative micrographs of this type of fault are shown in Fig. (V-1), in both image and diffraction, which were all recorded in the <310> pole.

With reference to the crystal structure of copper pthalocyanine (Fig. I-3(1) Fig. V-2a is seen to represent the (100) projection of the perfect structure whilst Fig. V-2b represents the same projection but of the faulted structure. Here and in other subsequent Figs. the white projected squares (reduced in size in the (100) projection but to scale in the (010) projection) represent the molecules of the orientation of the molecule at 000. The black squares represent molecules of the orientation of those molecules at the $\frac{1}{2}\frac{1}{2}0$ sites.

The orientation relationship between these two types of molecule is a (100) mirror plane. The presence of the $(00\frac{1}{2})$ reflection is therefore thought to arise because of the change in spacing of alternate pairs of (001) planes, caused by the differences in the nearest neighbor configuration in alternate planes.

Confirming evidence for the faulted structure was obtained by monitoring the lattice images under continued irradiation since the effect of radiation damage (Fig. V-3) is to degrade the coarse periodicity to half of its original spacing in both image and diffraction.

The additional planar faults visible in Figs. V-1 and V-3 are also consistent with the faulted structure explanation and are thought to arise from mis-stacking within the regular array that is present (Fig. V-2c).

That these $(00\frac{1}{2})$ lattice images and the associated faults lose contrast with continued irradiation and degenerate into a finer more regular lattice image (Fig. V-3) suggest that the distinguishableness of the alternate $(00\frac{1}{2})$ planes, which is due to the alternate orientation of molecules in the <110> direction, is lost. This degradation from a primitive monoclinic structure with two atoms per lattice point to c-centered monoclinic would be due to the relaxation of the molecules after degradation and possibly involves some rotation of the molecules within the damaged unit cell. In addition to the superperiodicity in the form of the $(00\frac{1}{2})$ lattice images, superperiodicities of the $(20\bar{1})$ (9.62 → 10.6Å) planes, the $(10\frac{\bar{1}}{2})$ (19.2 → 21.2Å) images have been observed and identified in the (102) pole. Similarly these can be

0 0 0 0 4 5 0 3 9 6 3

interpreted in terms of the same stacking faults but in the $(20\bar{1})$ planes, since again nearest neighbors of unlike orientation can be brought together. Such an interpretation however cannot account for the presence of broad faults within the $(20\bar{1})$ lattice images (Fig. V-4) which do not extend along the length of the transformed crystal.

The superperiodicity of the $(20\bar{1})$ planes can alternatively be formed however from the misstacking of (201) planes as is evident in Fig. V-5b where the alternate misstacking generates the alternate double planes of differently orientated molecules. The effect of a misstacking within this array, in the form of triplets along (201), is shown in Fig. V-5c. That these triplets, or the appropriate defect arising from an irregularity in the array, do not lie along a $(20\bar{1})$ plane means that their contrast will not be of the type observed in the (001) planes. In Fig. V-5d which represents a thin crystal some four molecules thick the presence of one stacking irregularity is some seven $(20\bar{1})$ planes broad and occurs at two different thicknesses within the foil. Similarly, thicker specimens will contain more defects at different depths extending over more $(20\bar{1})$ planes. Thickness differences along the crystal will determine the presence of the fault and it need not extend over the whole transformed length.

In addition to superperiodicities, stacking arrangements of the type shown in Fig. V-6 can cause changes in the average spacing of planes. This effect would be also evident in diffraction since the difference in spacing will cause a doubling of diffraction spots with an azithmal componant difference.

Figure V-7 is an example of a lattice image displaying such characteristics and the associated diffraction pattern. The pole is <100> and <010> is along the length of the crystal. The lattice fringes either side of the interface correspond to the (001) planes.

C. Discussion

That the general nature of these images can be explained in terms of the misstacking of alternately orientated molecules certainly substantiates the predictions that such stacking irregularities exist in similar crystals. Such faults could be responsible for certain products of solid state photodimerization (Thomas, 1974), where molecular orientations different from those sustained in the perfect crystal must be accounted for.

It is interesting to note that Ashida, Uyeda and Suito (1966), have, by electron diffraction, identified an α form of copper pthalocyanine with a C_2/c structure with lattice parameters of a = 29.52Å, b = 3.79Å, c = 23.92Å and β = 90.4°. The c spacing in this form being comparable to that resolved in the (001) type of transformed structure which if otherwise unchanged from the β form has lattice parameters a = 19.6Å, b = 4.79Å, c = 28.2Å, β = 120.6°. It is interesting to not however that the volume of the unit cell identified by Ashida et al is 2348 $Å^3$ compared to that of 2359 $Å^3$ for twice the unit cell volume of the β form and that with radiation damage the $(00\frac{1}{2})$ spacing decreases from 25.14Å to 23.4Å. This structure of the α form is in conflict with the data of Robinson and Klein (1952) who determined the α form to be probably $C^1_{4h} - P4/_m$ with a = 17.36Å and c = 12.79Å. Thus it is certainly

0 0 0 0 4 5 0 3 9 6 4

possible that more metastable forms of copper-pthalocyanine exist than have yet been predicted. The structure observed here however is apparent only in discrete portions of a crystal and will degrade with radiation damage to a structure consistent with the standard β-form within a very limited electron exposure.

It is apparent that the presence of such stacking modifications results in the generation of a distinctly different crystal structure and hence the generation of such modification represents a transformation of crystal structure. Quite obviously the orientation of the transformed to the parent phase is well defined and therefore in conflict with the exhaustive studies of Mnyukh (1963) and Kitaigorodsky (1965, 1975) who find that the orientation relationships between the transformed and parent regions are not well defined in organic crystals. Thomas (1974) conversely notes that in the monomeric 1,8-dichloro-10-methyl anthracene (Williams, 1973) all the symptoms of stress induced martensitic transformations are displayed with orientation relationships that are well defined between the daughter and parent phase.

The transformation product observed here could well be formed by a shear mechanism and the analogy it bears to the FCC-HCP transition in metals is clearly apparent when this mechanism is considered.

The simplest explanation for the formation of such a structure from the β form is in terms of the motions of partial dislocations of the type $\frac{1}{2}\langle 110\rangle$ (001) acting on every other glide plane. Thus if A represents an (001) plane and B the same plane displaced by such a dislocation we may represent the transformation in the notation commonly used in the description of partial dislocations, i.e.

A	A	A	A
A	A	A	A
A	A	A	A
$\vec{A}$	B	B	B
A	B	B	B
A	$\vec{B}$	A	A
A	B	A	A
A	B	$\vec{A}$	B
A	B	A	B

Thus the perfect structure projected onto (010) is shown in Fig. V-8a where the black rectangles represent molecules of different orientation from those in white. The identical stacking of the (001) planes is disturbed in Fig. V-8b by the passage of a partial dislocation (arrowed) of the form $\frac{1}{2}\langle 110\rangle$ (001) and a pair of adjacent planes where like molecules are not stacked on top of each other is generated. These layers where the original molecule at 000 (white) is replaced by one which usually appears at $\frac{1}{2}\frac{1}{2}0$ (black) is the B type. The passage of four such dislocations is shown in Fig. V-8c.

It is interesting to note the analogy of the predicted FCC HCP transition generated by the passage of $a/2\langle 11\bar{2}\rangle$ partial dislocations on alternate (111) planes in FCC, i.e.

0 0 0 0 4 5 0 3 9 6 5

A	A	A	A
B	B	B	B
C	C	C	C
A	B	B	B
B	C	C	C
C	A	B	B
A	B	C	C
B	C	A	B
C	A	B	C
A	B	C	A
B	C	A	B
C	A	B	C

Thus in both cases each dislocation introduces an antiphase boundary in its passage.

Similarly the stacking sequences predicted in the $(20\bar{1})$ planes can be generated by the passage of partial dislocations of the form $\frac{1}{2}\langle\bar{1}12\rangle$ (201) on every other glide plane. Figure V-5a shows the perfect structure projected onto (010) where again the convention of black and white projected squares is maintained. In Fig. V-5b the passage of partial dislocations (arrowed) of the form $\frac{1}{2}\langle\bar{1}12\rangle$ $(20\bar{1})$ can be seen to generate the associated structure with the appropriate spacing variations of alternate planes.

The stacking sequence responsible for the differently spaced lattice planes on either side of an interface Fig. V-7 can be generated by partial dislocations of the form $\frac{1}{2}\langle110\rangle$ (001) and again an analogy

with FCC metals can be cited since this stacking sequence can be generated by the passage of dislocations of this form on every plane, i.e.

A	A	A	A	A	A
A	A	A	A	A	A
A	A	A	A	A	A
A	A	A	A	A	A
A→	B	B	B	B	B
A	B→	A	A	A	A
A	B	A→	B	B	B
A	B	A	B→	A	A
A	B	A	B	A→	B
A	B	A	B	A	A

compared to the proposed twinning reaction in FCC metals on (111) planes, i.e.

A	A	A	A	A	A	A
B	B	B	B	B	B	B
C	C	C	C	C	C	C
A	A	A	A	A	A	A
B	B	B	B	B	B	---B---
C→	A	A	A	A	A	A
A	B→	C	C	C	C	C
B	C	A→	B	B	B	B
C	A	B	C→	A	A	A
A	B	C	A	B→	C	C

0 0 0 0 4 5 0 3 9 6 6

The effect of these arrowed dislocations on the (100) projection is shown in Fig. V-6b. The twin analogy is interesting since the effect is indeed to generate a psuedo twin which is apparent when the (010) projection of the crystal is considered (Fig. V-6c). This coincidental twin-like configuration may well account for the small rotation across the interface which is visible in the diffraction pattern of Fig. V-7.

The presence of dislocations in this material is indicated by the contrast features consistent with the predictions of Cockayne et al (1971) where in general terminating fringes are not observed. Thus in Fig. V-9b where the number of terminating fringes is zero if the N = g.b relation holds then $(20\bar{1})$ <hkl> = 0 and the burgers vector is $\frac{1}{n}$ <1k2>.

It is noteworthy that the vector ½<102> connects molecules of alternatively different orientation and is one of the six such vectors capable of introducing an antiphase boundary and is the partial dislocation predicted to account for one of the transformed structures. Defects where the number of terminating fringes is not zero have also been observed in the $(20\bar{1})$ lattice images. For example in Fig. V-9a three adjacent regions of lattice distortion are evident on top of each other in the [010] direction and are indicated by the intersection of the arrows. Here the burgers circuits taken within the indicated area show each region is associated with one terminating fringe and hence g.b = 1 = $(20\bar{1}) \cdot (hkl)$ which is consistent with a burgers vector of the form b = ½<110> which is predicted to be responsible for two other transformations observed.

It is well known that the associated displacement from the passage of a dislocation introducing an antiphase boundary involves the presence of a retarding force. Thus in an extended crystal the transformed region should be contained by two partial dislocations, constituting a "super-dislocation", the passage of the pair regenerating the perfect crystal structure. The presence of transformed and untransformed regions along a crystal is therefore predicted and these contrast features are observed (Fig. V-1). Certainly a large number of boundaries are observed in some crystals. Regions of preferential radiation damage, different focus and thickness variation could however, also contribute to this form of contrast.

Although the technique of defect characterization from lattice fringe behaviour is a well established technique it is difficult to perform in this material because the enclosure of a complete burgers circuit is usually difficult. Edge effects are prevalent because of the small dimensions of these crystals and the large lattice spacings tend to increase the problem further in terms of the requirements of wide crystals.

0 0 0 0 4 5 0 3 9 6 7

FIGURE CAPTIONS

Fig. V-1 The diffraction pattern (a) and image (b) from an (001) type stacking fault in copper pthalocyanine in the <310> pole. Regions of the perfect crystal structure are also visible along the same crystal (c).

Fig. V-2 The stacking sequences responsible for the (001) type stacking faults in copper pthalocyanine; (a) shows the perfect structure whilst (b) shows the new structure. The structure shown in (c) is an example of the type of structure expected when misstacking occurs, giving rise to the inconsistencies in the double spacing of Fig. V-1b. The views are along the a axis of the crystal.

Fig. V-3 Consecutive micrographs (a through d) taken from the same region of an (001) type stacking fault in copper pthalocyanine showing its disappearance under radiation damage. The micrographs involved electron exposures of about 10^{-1} C cm^{-2} to the specimen in their recording.

Fig. V-4 The diffraction pattern and image from a $(20\bar{1})$ type stacking fault in copper pthalocyanine in the <102> pole. A region of the perfect crystal structure is also visible further along the same crystal.

Fig. V-5 The stacking sequences responsible for the $(20\bar{1})$ type stacking faults in copper pthalocyanine; (a) shows the perfect structure whilst (b) shows the new structure. The structure shown in (c) is an example of the type of structure expected when misstacking occurs and d is the type of misstacking thought to give rise to the inconsistencies in the double spacing of Fig. V-4. The views are along the b axis of the crystal.

Fig. V-6 The stacking sequences thought to be responsible for the

structure observed in Fig. V-7 of copper pthalocyanine; (a) represents the perfect structure and (b) the faulted structure both viewed along the a axis of the crystal. (c) represents the faulted structure viewed along the b axis of the crystal.

Fig. V-7 The diffraction pattern and image from a twin-like interface in copper pthalocyanine. The crystal pole is <100>.

Fig. V-8 A possible mechanism for the formation of the <001> type stacking faults in copper pthalocyanine by the motion of partial dislocations of tye type $\frac{1}{2}$<110> (001). The perfect structure (a) is shown modified by the passage of one dislocation (b) and of four dislocations (c).

Fig. V-9 High resolution images from copper pthalocyanine showing (a) three dislocations within the $(20\bar{1})$ lattice images each displaying one terminating fringe and (b) a dislocation image within the $(20\bar{1})$ lattice images displaying no terminating fringe.

0 0 0 0 4 5 0 3 9 6 8

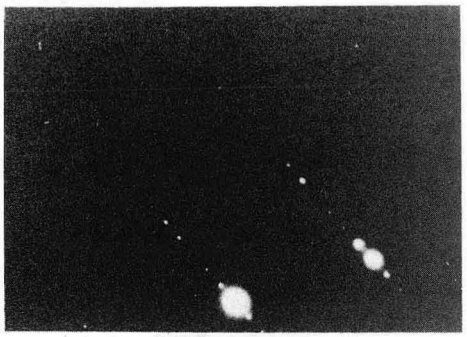

(a)

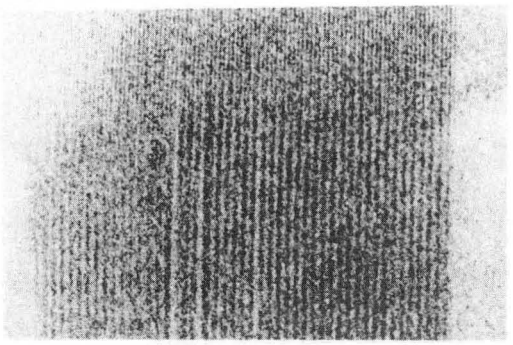

(b)

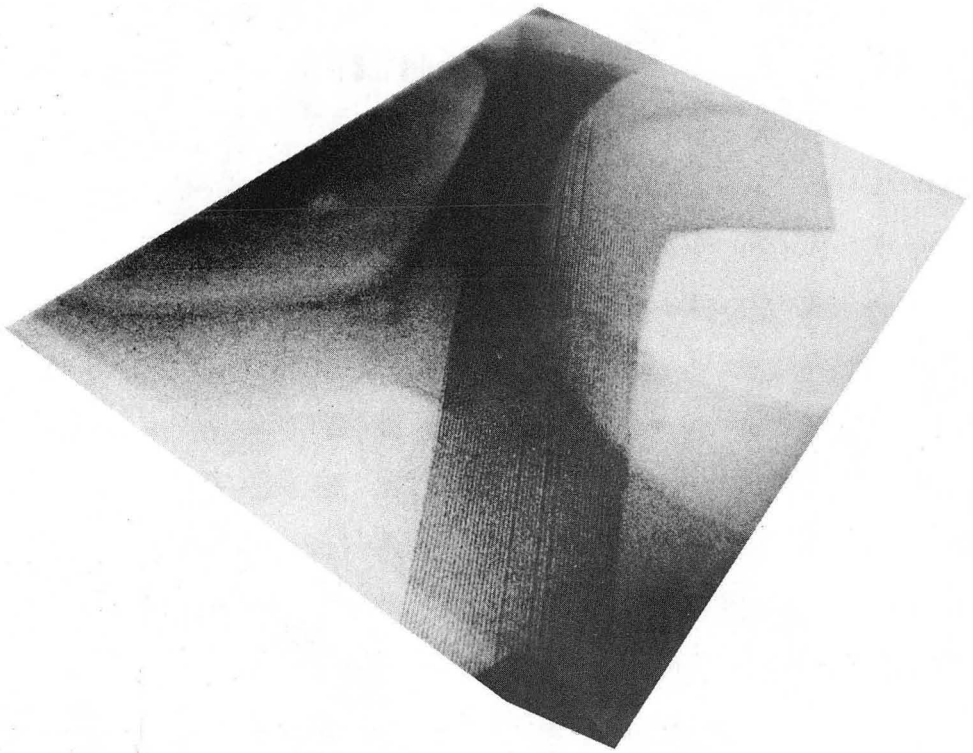

(c)

XBB765-4595

Fig. V-1

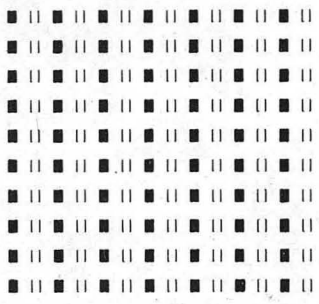

(a)

(b)

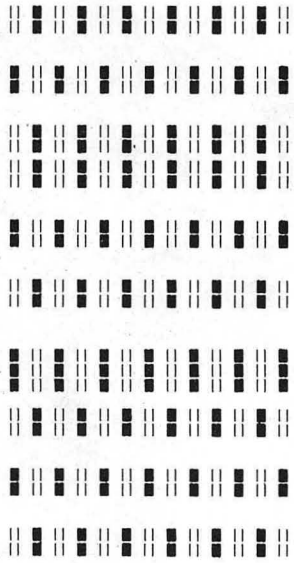

(c)

Fig. V-2

XBL 765-1952

0 0 0 0 4 5 0 3 9 6 9

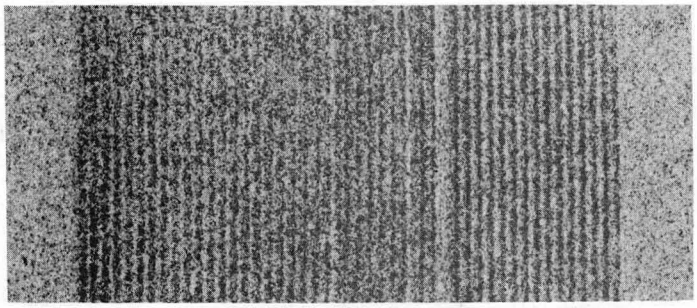

(a)

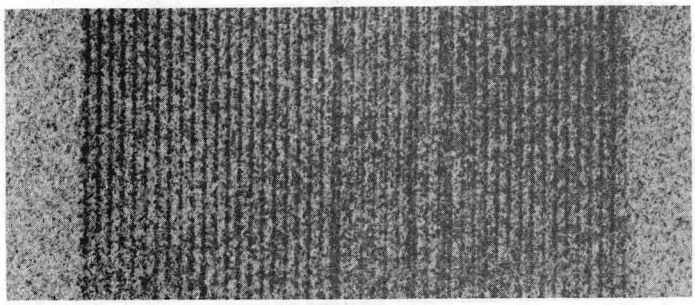

(b)

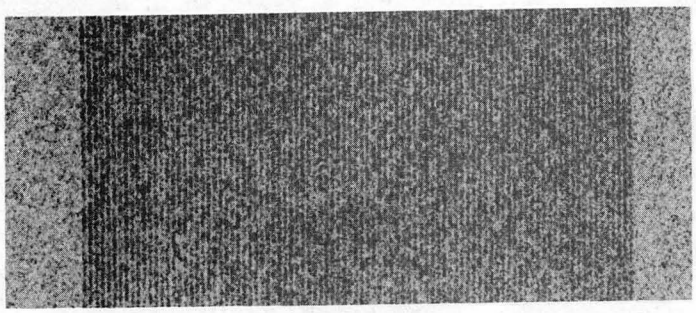

(c)

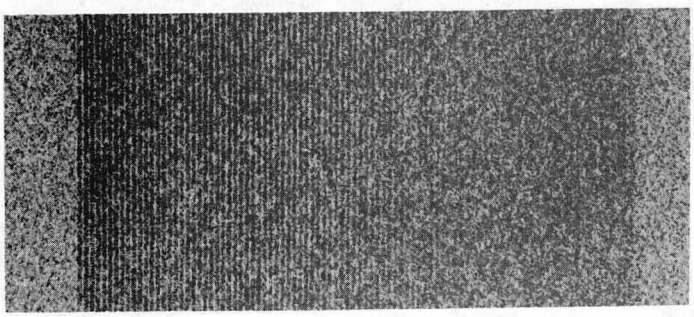

(D)

XBB755-3888

Fig. V-3

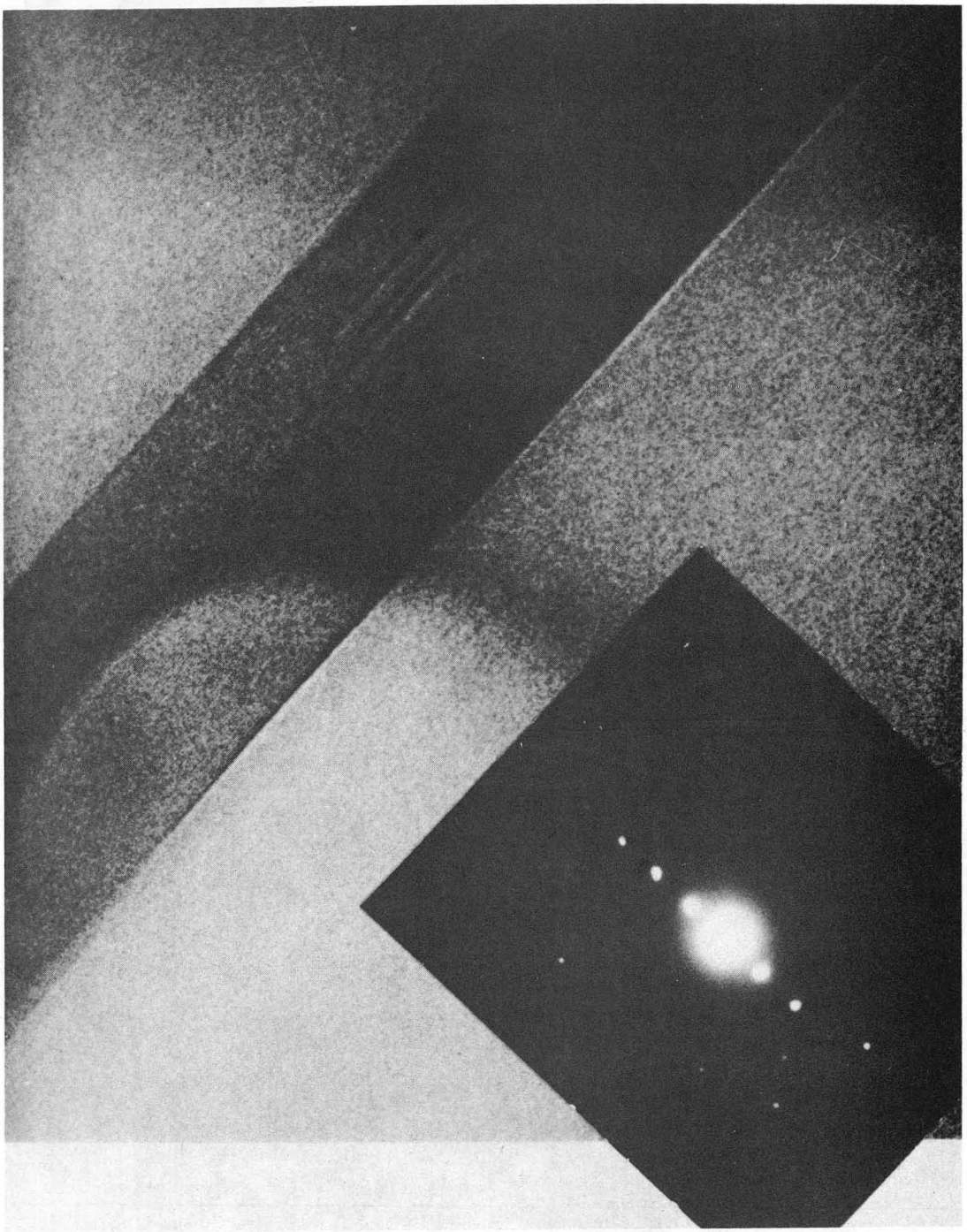

XBB755-3891-A

Fig. V-4

0 0 0 0 4 5 0 3 9 7 0

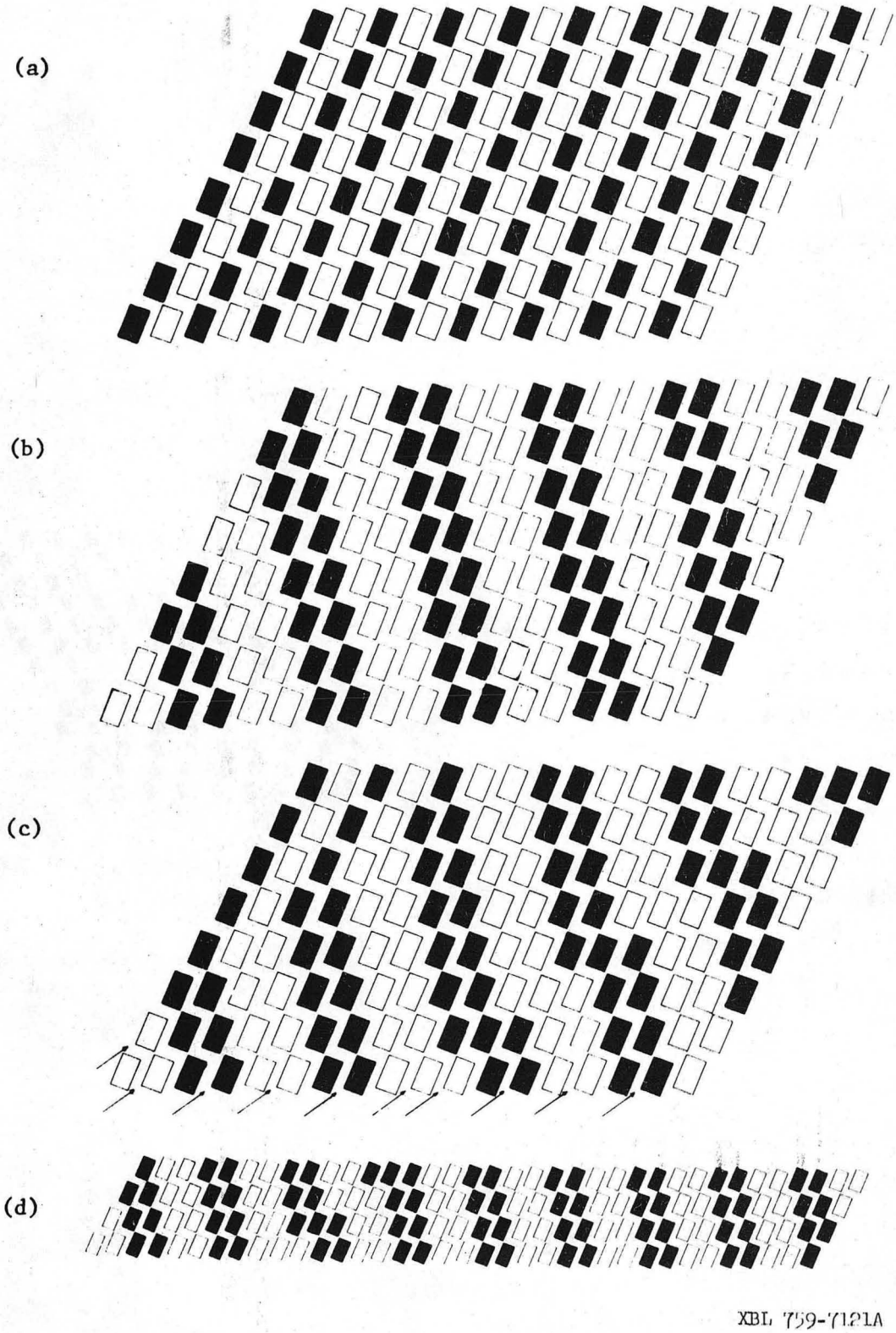

XBL 759-7121A

Fig. V-5

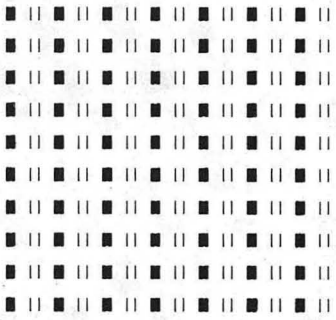

(a)

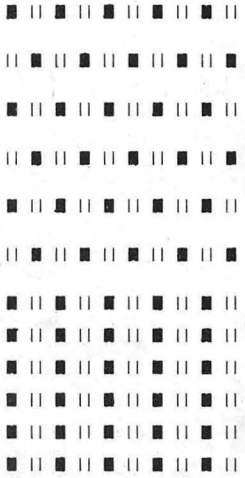

(b)

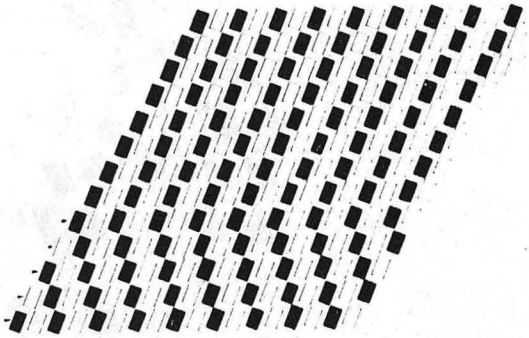

(c)

XBL 765 1953

Fig. V-6

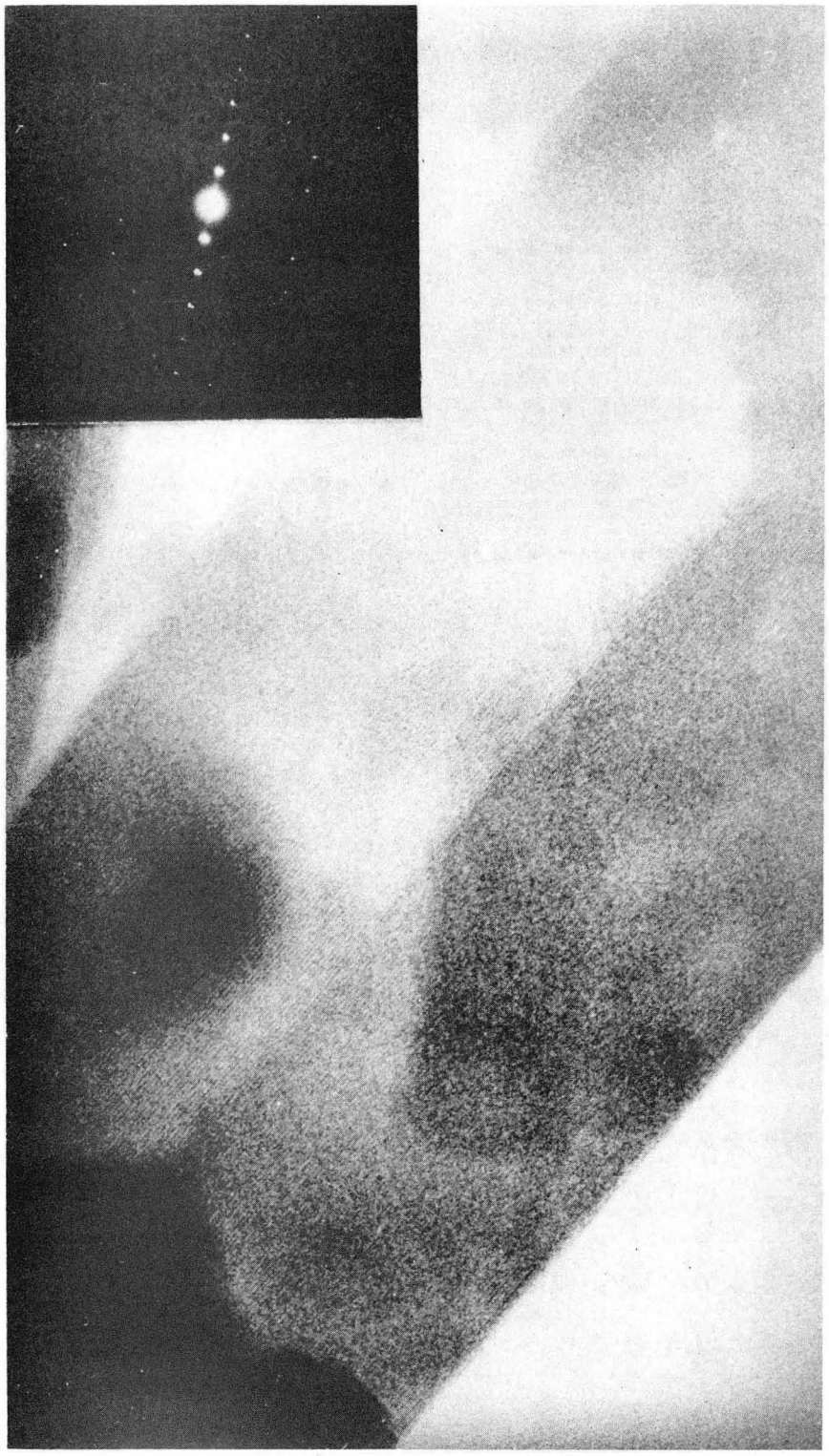

XBB758-6377-A

Fig. V-7

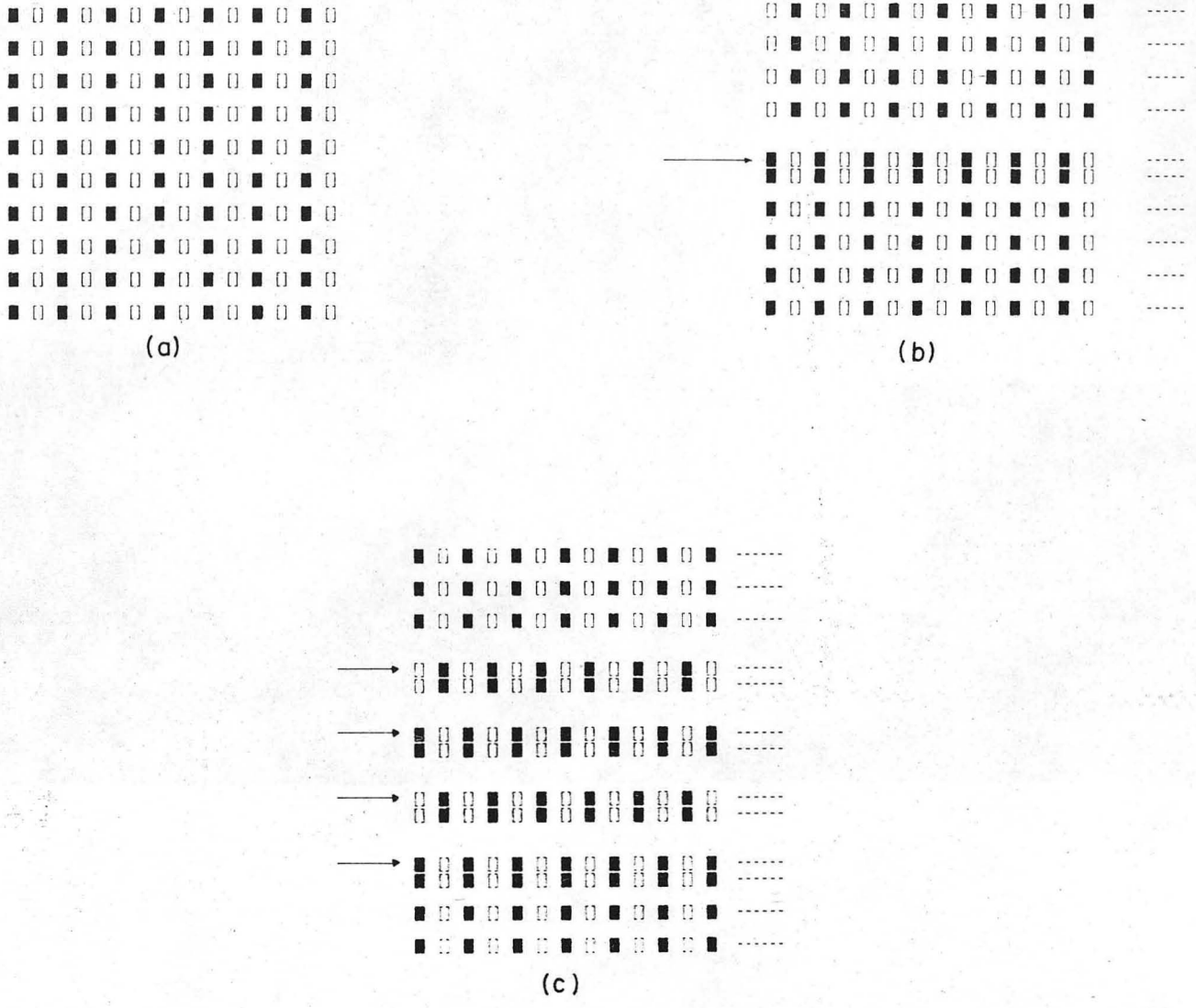

Fig. V-8

XBL 765-1954

0 0 0 0 4 5 0 3 9 1

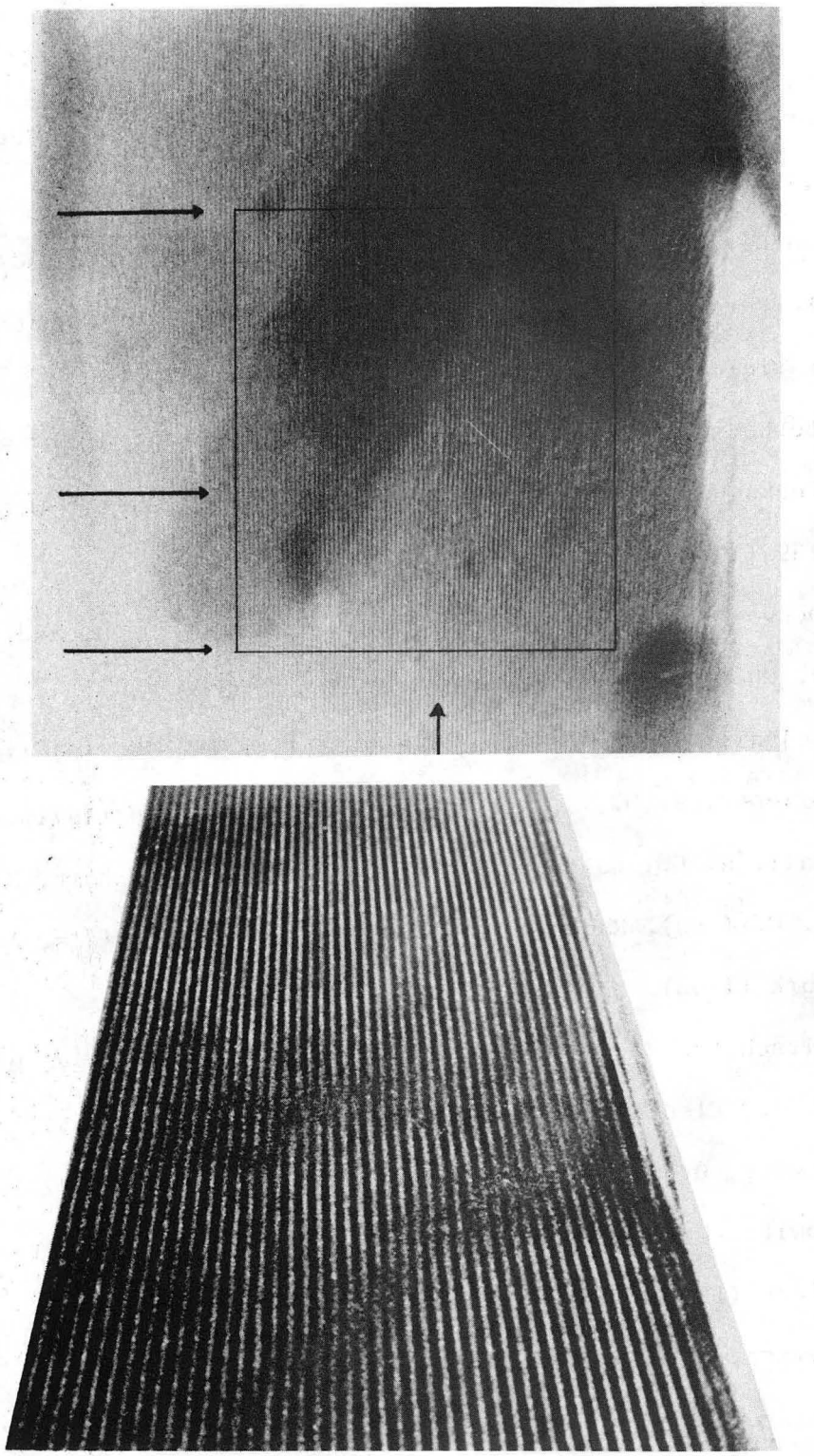

XBB758-5819-A

Fig. V-9

REFERENCES

Ashida, M., Uyeda, N., Suito, E., Bull Chem. Soc. Jap. 39, 12, 2616 (1966).

Barker, D. L. and Marsh, R. E., Acta Cryst. 17, 1581 (1964).

Berger, M. J. and Seltzer, S. M. in Studies of Penetration of Charged Paricles in Matter, NAS-NRC, Pub. 1133, 205 (1964).

Bethe, H. A. and Heitler, W., Proc. Roy. Soc. A146, 83 (1934).

Cockayne, D. J. H., Parsons, J. R. and Hoelke, C. W., Phil. Mag. 24, 139 (1971).

Desvergne, J. P., Thomas, J. M., Williams, J. O. and Bouas-Laurent, H., J. Chem. Soc. Perkin Trans. II 363 (1964).

Gejvall, T. and Lofroth, G., Rad. Effects, 25, 187 (1975).

Glaeser, R. M., J. Ultrastruct. Res., 36, 466 (1971).

Hall, K. L., Bolt, R. O. and Carrol, J. G. in Bolt, R. O. and Carrol, J. G. (eds), Radation Effects on Organic Materials, Academic Press, New York (1963).

Hirsch, P. B., Howie, A. Nicholson, R. E., Pashley, D. W. and Whelan, M. J., Electron Microscopy of Thin Crystals, (1965).

Howitt, D. G., M.S. Thesis, L.B.L. Report 3180 (1974).

Howitt, D. G., Glaeser, R. M. and Thomas, G., J. Ultrastruct. Res. in press (1976).

Howitt, D. G., Thomas, G. and Toutolmin, W., J. Appl. Phys. 47, 4 (1976).

Jeffrey, G. A. and Kinoshita, Y., Acta Cryst, 16, 20 (1963).

Jones, W., Thomas, J. M. and Williams, J. O. Phil. Mag., 32, 1, 1, (1975).

Jones, W., Thomas, J. M., Williams, J. O. and Hobbs, L. W., J. Chem. Soc. Farad. Trans. II, 71, 138 (1975).

Kilaigorodsky, A. I., Acta Cryst., 18, 588 (1965).

Kilaigorodsky, A. I., Molecular Crystals and Molecules, Academic Press, New York, (1973).

Magee, J. L., J. Am. Chem. Soc., 73, 3270 (1951).

Menter, J. W., Proc. Roy. Soc. A236, 119 (1956).

Mnyukh, Y. U., J. Phys. Chem. Solids, 24, 631 (1963).

Newton, A. S. in Bolt R. O. and Carrol, J. G. (eds). Radiation Effects on Organic Materials, Academic Press, New York (1963).

Parsons, D. F., Matricardi, V. R., Moretz, R. C. and Turner, J. N., in Adv. in Bio. and Med. Phys., 15, 162. Academic Press, New York (1974).

Rauth, A. M. and Simpson, J. A., Rad. Res. 22, 643 (1964).

Reicke, W. D., Z. Agnew. Phys., 27, 155 (1969).

Reimer, L., Lab. Invest., 14, 1082 (1965).

Robertson, J. M., J. Chem. Soc. 615 (1935).

Robertson, J. M. and Woodward, I., J. Chem. Soc, 219 (1937).

Robinson, M. T., Klein, G. E., J. Am. Chem. Soc., 74, 6294 (1952).

Salih, S. M. and Cosslett, V. E., Phil. Mag., 30, 1, 225 (1974).

Seitz, F. and Koehler, J. S. in Seitz, F. and Turnball, D. (eds). Displacement of Atoms During Irradiation, Academic Press, New York, Vol. II, 330 (1956).

Taylor, K. A. and Glaeser, R. M., Science, 186, 1036 (1974).

Thomas, J. M., Phil. Trans. R. Soc. Lond. A, 277, 251 (1974).

Thomas, J. M. and Williams, J. O., in Surface and Defect Properties of Solids, 1, 130 (1972).

Torri, K. and Iitaka, Y., Acta Cryst., B26, 1317 (1970).

Williams, J. O., J. Matl. Sci, 8, 1361 (1973).

Williams, R. C. and Fisher, H. W., J. Molec Biol. 52, 121 (1970).

VI. SUMMARY

The role of high resolution electron microscopy in the study of molecular organic materials has been reported.

It has been shown that the effects of radiation damage are predictable when the degradation pathway of the material is known and that the effects of radiation damage on the stability of certain types of microstructure can be estimated qualitatively.

The predicted structural features of radiation damage have been identified and in addition changes in crystal structure induced by radiation damage have been reported.

In copper pthalocyanine it has also been shown that a variety of planar faults exist, representing transformed regions that sustain an uniquely defined orientation relationship to the parent phase. These faulted regions, and the two phase structures they induce are identifiable only by electron microscopy and are possibly responsible for some of the crystal structures that have been previously identified as single phase.

A model for the formation of these structures has been presented which is closely analagous to those thought to be responsible for certain shear transformations in metallic systems.

ACKNOWLEDGMENTS

It is with gratitude that I acknowledge the supervision and instigation of this project by Professor Gareth Thomas and the extensive contributions made by Professor Robert Glaeser.

For financial support I thank both the U. S. Energy Research and Development Administration and the National Institute of Health.

For preparation of the manuscript I thank Betty Rancatore, Diane Kaufman, Rebecca Gloff and Shirley Ashley and for the preparation of figures Gloria Pelatowski and Marty Pike.

I am particularly grateful to Krishna Seshan, Omer Van der Biest and Roy Geiss for their discussions and to my wife Sheila, I remain forever in her debt.

0 0 0 0 4 5 0 3 9 7 2

This report was done with support from the United States Energy Research and Development Administration. Any conclusions or opinions expressed in this report represent solely those of the author(s) and not necessarily those of The Regents of the University of California, the Lawrence Berkeley Laboratory or the United States Energy Research and Development Administration.

TECHNICAL INFORMATION DIVISION
LAWRENCE BERKELEY LABORATORY
UNIVERSITY OF CALIFORNIA
BERKELEY, CALIFORNIA 94720